

## Mathematical modelling of avascular-tumour growth II: Modelling growth saturation

J. P. WARD AND J. R. KING

*Department of Theoretical Mechanics, University of Nottingham,  
Nottingham, NG7 2RD, UK*

[Received 19 December 1997 and in revised form 5 June 1998]

We build on our earlier mathematical model (Ward & King, 1997, *IMA J. Appl. Math Appl. Med. Biol.*, **14**, 39–69) by incorporating two necrotic depletion mechanisms, which results in a model that can predict all the main phases of avascular-tumour growth and heterogeneity. The model assumes a continuum of live cells which, depending on the concentration of a generic nutrient, may reproduce or die, generating local volume changes and thus producing movement described by a velocity field. The necrotic material is viewed as basic cellular material (i.e. as a generic mix of proteins, DNA, etc.) which is able to diffuse and is utilized by living cells as raw material to construct new cells during mitosis. Numerical solution of the resulting system of partial differential equations shows that growth ultimately tends either to a steady-state (growth saturation) or becomes linear. Both the travelling-wave and steady-state limits of the model are therefore derived and studied. The analysis demonstrates that, except in a very special case, passage of cellular material across the tumour surface is necessary for growth saturation to occur. Using numerical techniques, the domains of existence of the large-time solutions are explored in parameter space. For a particular limit, asymptotic analysis makes explicit the main phases of growth and gives the location of the bifurcation between the long-time outcomes.

*Keywords:* tumour growth; mathematical modelling; numerical solution; asymptotic analysis.

### 1. Introduction

The growth of tumours can be divided into two main phases, namely avascular and vascular. Initially the nutrient (oxygen, glucose, etc.) supplied by diffusion from the existing vasculature is adequate for growth and it is this avascular stage that we consider here. An *in vitro* analogue for tumour growth is provided by multicell spheroid cultures, produced by growing colonies of cells suspended in a nutrient matrix. The growth of multicell spheroids is determined mainly by the extent of nutrient penetration by diffusion from the growth matrix. Growth starts off by being exponential due to all cells being adequately nourished, but retards to a linear growth phase due to a developing region of quiescent cells and necrosis in the core (Congar & Ziskin, 1983). Following the linear phase, growth retards further ultimately reaching a saturation level at which it apparently ceases (Inch *et al.*, 1970; Folkman & Hochberg, 1973; Carlsson, 1977). The saturated spheroid has a characteristic three-layered structure consisting of an outer rim of adequately nourished reproducing cells, an intermediate layer of quiescent cells and a relatively large central necrotic core (Freyer & Schor, 1989).

In an earlier paper (Ward & King, 1997) a mathematical model for the growth of avascular (spheroid) tumours is proposed and studied in detail. This model succeeds in capturing the first two stages of growth, namely the initial (exponential) and the intermediate (linear) phases. The lack of any growth-retardation mechanism, other than volume loss at cell death, means that a saturation state is never attained, except in the special case of zero dead-cell volume. This continued growth results from the products of cell death remaining within the spheroid without decaying or escaping, with the living cells continually adding to the volume through cell birth. Despite this deficiency, the analysis offers insight into key characteristics of growth such as the time scales on which exponential growth ceases and on which necrosis starts and length scales for the proliferating and quiescent layers. In the special case of zero dead-cell volume, the resultant saturated spheroid consists entirely of living cells, lacking a necrotic core, which contradicts experimental observation. The aim in this paper is to extend this model by employing physical mechanisms that can result in growth saturation.

Although there are several studies investigating the effects of environmental factors on the eventual saturation size (Mueller-Klieser *et al.*, 1985; Freyer & Sutherland, 1986; Tanock & Kopelyan, 1986a,b), there is very little information on what actually causes the saturation of growth. Mitotic inhibitors have been extracted from the necrotic core (see, for example, Freyer, 1988; Levine *et al.*, 1984), and these presumably diffuse through the spheroid affecting the mitotic behaviour of some of the cells; however, this mechanism alone cannot be responsible for saturation since it requires that all the cells be completely inhibited from dividing if a continued increase in volume due to cell reproduction is to be prevented, contradicting experimental observation. During mitosis, the reduced strength of the binding between cells may cause individual cells to be shed into the surrounding matrix (Landry *et al.*, 1981; Weiss, 1978); however, the cells that remain will still reproduce, so this mechanism on its own cannot explain growth saturation either, unless all new born cells are ultimately shed. The processes of mitotic inhibition (see Greenspan, 1972; Shymko & Glass, 1976; Adam, 1986) and cell shedding (see Landry *et al.*, 1982; Casciari *et al.*, 1992) have been studied extensively using mathematical models. These aspects have also been incorporated into an extension of the model proposed here and are discussed in Ward (1997); this will be the subject of a future publication. Mathematical models that predict the saturation phase have, as their crucial assumption, a continual process of necrotic-volume loss. They typically include an expression whereby either the necrotic core contracts (Greenspan, 1972; Maggelakis & Adam, 1990) or the viable regions contract, reflecting apoptosis (McElwain & Morris, 1978; Byrne & Chaplain, 1995) or a combination of these processes (Byrne & Chaplain, 1996). The terms introduced to model contraction are somewhat *ad hoc* and are intended to represent the disintegration of necrotic material or the breakdown products of apoptosis into simpler permeable compounds which quickly diffuses out of the tumour, with a subsequent loss in its volume. This approach to modelling necrotic-volume loss, while simplistic, makes the resulting model more tractable. However, such models provide little understanding of the manner in which the material is lost.

In this paper it is assumed that cells require basic cellular material (such as proteins, DNA, and lipids), as well as nutrients, in order to reproduce. This cellular material is provided by the breakdown products of necrosis and by the external medium (neighbouring tissues *in vivo* or the growth medium *in vitro*); for simplicity the material from the two

sources is here treated as being the same. Two pathways for the depletion of the cellular material, causing volume loss, result from the mechanisms proposed; the first involves the leakage of the cellular material by diffusion to the external matrix and the second involves the consumption of cellular material for the construction of new cells. Evidence related to the latter mechanism is given in Kerr *et al.* (1987), where neighbouring cells are observed to consume cells that have undergone apoptosis. It is anticipated that typically smaller molecules may leak out, whereas larger ones (with relatively low diffusivities) will be consumed. A natural development to the current model (Ward, 1997) accounts for two distinct species, but the resulting behaviour is qualitatively similar to that described below. The basic approach to the modelling in this paper follows that of Ward & King (1997) and is based on the assumption that the tumour consists of a continuum of cells; depending on the local nutrient concentration, volume changes through cell birth and death generate a velocity field in the tumour, so the role of convection needs to be considered. In the next section the details of the necrotic volume-loss mechanisms are given and the model is derived in terms of a system of partial differential equations, with spherical symmetry assumed. The numerical solutions in Section 3 demonstrate that the long-time outcomes can either be growth saturation or linear growth, depending on the parameters' values. These long-time outcomes are studied in detail in Sections 4 and 5, where the steady-state and travelling-wave limits of the model are derived and studied. In Section 4 it is established that, except in a special case, passage of material across the spheroid surface is a necessary condition for growth saturation. Conditions for the bifurcation between the two types of long-time behaviour are established and, in the numerical solutions of Section 5, the regions of existence of these solutions in parameter space are determined.

**2. Model formulation**

On the death of a cell, its constituents are assumed to immediately dissociate into necrotic material which is free to diffuse through the tumour. The necrotic products include basic cellular material (such as DNA, proteins, water, and lipids) which can be utilized by the living cells to construct new ones. Assuming the volume of a molecule of the (generic) basic cellular material to be  $V_p$ , we have

$$\mu V_p = V_D, \tag{1}$$

where  $V_D$  is the volume of a dead cell and the dimensionless constant  $\mu$  is the number of these molecules released at cell death. It is assumed that the time scale for this dissociative process is very much shorter than that of tumour growth. For mitosis it is assumed that a total volume of  $\lambda V_p$  of cellular material is required, which leads to the expression

$$\text{volume change during mitosis} = V_L - \lambda V_p, \tag{2}$$

where the constant  $V_L$  is the average volume of a living cell and the dimensionless constant  $\lambda$  is the number of molecules consumed. Here, for simplicity, we treat the time scale for the growth phase of each cell as small compared to that of the complete cell cycle. For there to be no voids in the tumour, with all space being occupied by either the living cells or cellular material, we require the no-void condition

$$V_L n + V_p p = 1, \tag{3}$$

where  $n$  and  $p$  are the concentrations of the living cells and the cellular material, respectively. We note that  $p$  is related to the concentration of necrotic material  $m$ , used in the model of Ward & King (1997), by  $m = p/\mu$ .

Using the above relations and the assumptions of Ward & King (1997), the following system of equations can be derived:

$$\frac{\partial n}{\partial t} + \nabla \cdot (vn) = [k_m(c, p) - k_d(c)]n, \quad (4)$$

$$\frac{\partial c}{\partial t} + \nabla \cdot (vc) = D\nabla^2 c - k(c, p)n, \quad (5)$$

$$\frac{\partial p}{\partial t} + \nabla \cdot (vp) = D_p \nabla^2 p + \mu k_d(c)n - \lambda k_m(c, p)n, \quad (6)$$

$$\nabla \cdot v = (V_L - \lambda V_p)k_m(c, p)n - (V_L - V_D)k_d(c)n + V_p D_p \nabla^2 p, \quad (7)$$

where  $c$  is the nutrient concentration and  $v$  is the velocity field. Equation (4) states that the rate of change in live-cell density is the difference in birth  $k_m(c, p)$  and death  $k_d(c)$  rates, the form of which are given below. We have also assumed that the cell-cell contacts are sufficiently strong that cell motion by diffusion or chemotaxis is negligible. The evolution of the nutrient concentration is given by (5), where Fick's law for diffusion is assumed to apply (with a constant diffusion coefficient  $D$ ) and the nutrient is consumed by the living cells at a rate  $k(c, p)$ , given below. The diffusion of the cellular material is also assumed to satisfy Fick's law, with constant coefficient  $D_p$ , and its generation and consumption are determined by expressions (1) and (2), yielding equation (6). The velocity field equation (7) involves the volume generated by birth, that consumed on death, and that transferred by the diffusion of the cellular material; it can be derived from equations (3), (4), and (6). In the application of radial symmetry in the spheroidal geometry adopted below, equations (4)–(7) suffice for a closed system, so the further constitutive relations needed to determine the velocity field for multidimensional problems are not required.

Since cellular material needs to be present for new cells to form we postulate that the mitotic rate is dependent on  $p$ . It is assumed that  $k_m(c, p)$  is bounded and monotonic increasing in both  $c$  and  $p$ , such that  $k_m = 0$  when  $c = 0$  or  $p = 0$ . To capture this type of dependence on  $c$  and  $p$ , we extend the form for  $k_m$  adopted in Ward & King (1997), again using a Michaelis–Menten-type expression, to

$$k_m(c, p) = A \left( \frac{c^{m_1}}{c_c^{m_1} + c^{m_1}} \right) \left( \frac{p^{m_3}}{p_c^{m_3} + p^{m_3}} \right), \quad (8)$$

where  $c_c$  and  $p_c$  are critical nutrient and cellular material concentrations, respectively, and the exponents  $m_1$  and  $m_3$  are non-negative constants which govern the sharpness of change of  $k_m$  around these critical concentrations. We again adopt the expression given in Ward & King (1997) for the death-rate concentration  $k_d(c)$ , namely

$$k_d(c) = B \left( 1 - \sigma \frac{c^{m_2}}{c_d^{m_2} + c^{m_2}} \right), \quad (9)$$

where  $B$ ,  $\sigma$ ,  $c_d$ , and  $m_2$  are non-negative constants, with  $\sigma \leq 1$ . The expression used for

$k$  in Ward & King (1997), namely  $k(c) = \beta k_m(c)$ , was based on experimental results suggesting that the consumption rate is approximately proportional to the mitotic rate. However, such experimental results are generally obtained from monolayer cultures in agar, where the concentrations of non-nutrient constituents are presumably kept relatively constant, effectively keeping  $p$  constant. Consequently, the effects of cellular material concentration are not known. However, quiescent cells presumably continue to metabolize nutrients in order to remain viable, and it is also envisaged that additional nutrient consumption will occur during mitosis. These ideas can be combined to yield the expression

$$k(c, p) = A \left( \frac{c^{m_1}}{c_c^{m_1} + c^{m_1}} \right) \left[ \beta_1 + \beta_2 \left( \frac{p^{m_3}}{p_c^{m_3} + p^{m_3}} \right) \right], \tag{10}$$

where  $\beta_1$  and  $\beta_2$  are positive constants, so that  $A(\beta_1 + \beta_2)$  is the maximum possible rate of consumption. We thus assume the necrotic material is consumed only by mitosis.

We exploit the spherical symmetry of the problem and restrict our attention to studying this system of equations in a single spatial variable  $r = |\mathbf{x}|$  with radial velocity  $v = |\mathbf{v}|$ . The initial state of the spheroid is a matter of choice but, in most of the simulations to follow, we commence with a single cancerous cell. The medium in which the spheroid grows is assumed partly to contain cellular material at a fixed concentration  $p_0$ , with the rest of space occupied by a nondiffusing material that takes no part in spheroid growth. The growth medium in which spheroids grow is frequently renewed and stirred in experiments (for example, daily in Freyer & Sutherland, 1980), so setting the external concentration of  $p$  to some constant  $p_0$  is probably reasonable. The initial and boundary conditions for  $n$ ,  $c$ , and  $v$  are as those in Ward & King (1997), and the complete set is

$$\begin{aligned} \text{at } t = 0 \quad & n = 1/V_L, \quad p = 0, \quad S = (3V_L/4\pi)^{1/3}, \\ \text{at } r = 0 \quad & \frac{\partial c}{\partial r} = \frac{\partial p}{\partial r} = v = 0, \\ \text{at } r = S \quad & c = c_0, \quad D_p \frac{\partial p}{\partial r} = Q_p(p_0 - p), \quad \frac{dS}{dt} = v, \end{aligned} \tag{11}$$

where the radius of the spheroid,  $S(t)$ , changes in time, being the coordinate of a moving boundary. We have imposed a Robin-type boundary condition for  $p$  at  $r = S(t)$ , which assumes that the flux of cellular material is proportional to the concentration difference there, the mass-transfer coefficient  $Q_p$  being a non-negative constant. For  $Q_p > 0$ , the cellular material is free to cross through the spheroid surface, so leakage (whereby  $\partial p/\partial r < 0$ ) will be a possible source of necrotic-volume loss.

We note that equations (4)–(10) generalize the model of Ward & King (1997), which corresponds to the special case  $D_p = 0$ ,  $p_c = 0$ ,  $\lambda = 0$ ,  $\beta = \beta_1 + \beta_2$ , and  $m = p/\mu$ . For the remainder of this paper we shall use the no-voids condition (3) to eliminate  $p$  using  $p = (1 - V_L n)/V_p$ , thus focusing on the live-cell density.

### 2.1 Nondimensionalization

Denoting dimensionless quantities by carets, we introduce the following rescalings which are based on the initial conditions:

$$n = \hat{n}/V_L, \quad c = c_0 \hat{c}, \quad v = r_0 A \hat{v}, \quad t = \hat{t}/A, \quad r = r_0 \hat{r}, \quad S = r_0 \hat{S},$$

where  $r_0 = S(0) = (3V_L/4\pi)^{1/3}$ . We note that this scaling for  $\hat{n}$  implies that for physically meaningful solutions we must have  $0 \leq \hat{n} \leq 1$ . We will adopt the quasisteady simplification for  $c$  for the reasons detailed in Ward & King (1997) and the full system of nondimensional equations can then be written as

$$\frac{\partial \hat{n}}{\partial \hat{t}} + \hat{v} \frac{\partial \hat{n}}{\partial \hat{r}} = \hat{n} \frac{\hat{D}_p}{\hat{r}^2} \frac{\partial}{\partial \hat{r}} \left( \hat{r}^2 \frac{\partial \hat{n}}{\partial \hat{r}} \right) + [a(\hat{c}, 1 - \hat{n}) - b(\hat{c}, 1 - \hat{n}) \hat{n}] \hat{n}, \quad (12)$$

$$\frac{1}{\hat{r}^2} \frac{\partial}{\partial \hat{r}} \left( \hat{r}^2 \frac{\partial \hat{c}}{\partial \hat{r}} \right) = \hat{k}(\hat{c}, 1 - \hat{n}) \hat{n}, \quad (13)$$

$$\frac{1}{\hat{r}^2} \frac{\partial (\hat{r}^2 \hat{v})}{\partial \hat{r}} = b(\hat{c}, 1 - \hat{n}) \hat{n} - \frac{\hat{D}_p}{\hat{r}^2} \frac{\partial}{\partial \hat{r}} \left( \hat{r}^2 \frac{\partial \hat{n}}{\partial \hat{r}} \right), \quad (14)$$

where  $\hat{D}_p = D_p/r_0^2 A$ . We note from (12) that the diffusion of the cellular material leads to a nonlinear degenerate diffusion term for  $n$ . The nonlinearity occurs because in the quantity  $n \nabla \cdot \mathbf{v}$ , representing the rate of change of  $n$  due to local volume creation or loss, part of the dilatation rate  $\nabla \cdot \mathbf{v}$  is due to the diffusion of cellular material, with (in view of (3))  $\nabla^2 p = -V_L \nabla^2 n / V_p$ . It will be shown that the nonlinearity in the diffusion term leads to the possibility of the solutions becoming degenerate in the core as  $t \rightarrow \infty$ . It should be stressed that this apparent diffusion of the living cells is a consequence of the modelling assumptions concerning the velocity field and is not due to cells being independently mobile.

The dimensionless functions  $a$  and  $b$  have the same interpretation as in Ward & King (1997) and are given by

$$a(\hat{c}, 1 - \hat{n}) = \hat{k}_m(\hat{c}, 1 - \hat{n}) - \hat{k}_d(\hat{c}), \quad (15)$$

$$b(\hat{c}, 1 - \hat{n}) = (1 - \hat{\lambda}) \hat{k}_m(\hat{c}, 1 - \hat{n}) - (1 - \delta) \hat{k}_d(\hat{c}), \quad (16)$$

where  $\delta = V_D/V_L = \mu V_p/V_L$ ,  $\hat{\lambda} = \lambda V_p/V_L$ ;  $a$  gives the overall birth rate and  $b$  the rate of volume change due to cell birth and death. The dimensionless quantities  $\hat{k}_m$  and  $\hat{k}_d$  are defined as

$$\hat{k}_m(\hat{c}, 1 - \hat{n}) = \left( \frac{\hat{c}^{m_1}}{\hat{c}^{m_1} + \hat{c}_c^{m_1}} \right) \left( \frac{(1 - \hat{n})^{m_3}}{\hat{p}_c^{m_3} + (1 - \hat{n})^{m_3}} \right),$$

$$\hat{k}_d(\hat{c}) = \frac{B}{A} \left( 1 - \sigma \frac{\hat{c}^{m_2}}{\hat{c}^{m_2} + \hat{c}_d^{m_2}} \right),$$

where  $\hat{p}_c = V_p p_c$ . The dimensionless consumption-rate function  $\hat{k}$  is now

$$\hat{k}(\hat{c}, 1 - \hat{n}) = \left( \frac{\hat{c}^{m_1}}{\hat{c}^{m_1} + \hat{c}_c^{m_1}} \right) \left[ \hat{\beta}_1 + \hat{\beta}_2 \left( \frac{(1 - \hat{n})^{m_3}}{\hat{p}_c^{m_3} + (1 - \hat{n})^{m_3}} \right) \right],$$

where  $\hat{\beta}_1 = r_0^2 \beta_1 A / D V_L c_0$  and  $\hat{\beta}_2 = r_0^2 \beta_2 A / D V_L c_0$ , where we recall that  $c_0$  is the external nutrient concentration. We note that the definitions of  $\hat{\lambda}$  implies that if it is greater than unity then there is an overall loss in volume during mitosis.

The dimensionless initial and boundary conditions are

$$\begin{aligned}
 &\text{at } \hat{t} = 0 && \hat{n} = 1, \hat{S} = 1, \\
 &\text{at } \hat{r} = 0 && \frac{\partial \hat{n}}{\partial \hat{r}} = 0, \frac{\partial \hat{c}}{\partial \hat{r}} = 0, \hat{v} = 0, \\
 &\text{at } \hat{r} = \hat{S}(\hat{t}) && \hat{c} = 1, \hat{D}_p \frac{\partial \hat{n}}{\partial \hat{r}} = \hat{Q}_p(1 - \hat{p}_0 - \hat{n}), \frac{d\hat{S}}{d\hat{t}} = \hat{v},
 \end{aligned} \tag{17}$$

where  $\hat{Q}_p = Q_p/r_0A$  and  $\hat{p}_0 = V_p p_0$ , so that  $\hat{p}_0 \leq 1$ .

The system (12)–(14) thus consists of a nonlinear diffusion–convection equation (12), a second-order differential equation (13), and a first-order partial differential equation (14), defined on a domain  $0 < \hat{r} < \hat{S}(\hat{t})$  with an unknown moving boundary  $\hat{S}(\hat{t})$ . It is well known that equations with degenerate nonlinear diffusion terms, such as occurs in (12), may have solutions with compact support. This phenomenon will be shown to occur for this system as  $\hat{t} \rightarrow \infty$  and is discussed in greater detail in Sections 4 and 5.

The model contains two mechanisms for the depletion of necrotic material, namely leakage by diffusion and consumption in mitosis. Each of these mechanisms can be switched off by an appropriate choice of parameters, as follows

(i) *Leakage only.* Setting  $\hat{p}_c = 0$  and  $\hat{\lambda} = 0$  prevents the utilization of the cellular material in mitosis. It will be shown that these conditions lead to either growth saturation or travelling-wave solutions.

(ii) *Consumption only.* Setting  $\hat{Q}_p = 0$ ,  $\hat{p}_c > 0$ , and  $\hat{\lambda} > 0$  ensures no passage of cellular material through the spheroid surface. The same effect can be achieved if we set  $\hat{D}_p = 0$ , which reduces the order of the system and requires that the boundary conditions for  $\hat{n}$  be dropped. Since in this case the only sources of cellular material are the products of necrosis, the initial condition  $\hat{n} \equiv 1$  leads to the peculiar situation that cell death is required for cells to start reproducing. In fact, the analysis of the long-time behaviour described in Section 4.5 shows that for  $\lambda < \delta$  travelling-wave solutions will result, while for  $\lambda > \delta$  the tumour dies out; however, an infinite number of steady-state solutions exist for  $\lambda = \delta$ , the amounts of material produced at cell death and used during mitosis then being the same. This can be illustrated by the special case  $\lambda = \delta = 1$ , where we have  $d\hat{S}/d\hat{t} = 0$  for all  $\hat{t}$ , so the resulting steady-state solution size will be the initial size. We stress that these comments are restricted to the consumption-only case.

It is clear from the assumptions adopted in constructing the model that, as well as cell birth and death, the absorption and diffusion of cellular material are key factors in determining the growth of the spheroid. This can be illustrated by considering the example  $\delta = \lambda = 1$ , in this case there being no volume loss at cell death, with exactly a cell-size volume of material being required to construct a new cell at mitosis. Integration of (14) using (17) then yields

$$\frac{d\hat{S}}{d\hat{t}} = \hat{D}_p \frac{\partial \hat{n}}{\partial \hat{r}}(\hat{S}, \hat{t}) = \hat{Q}_p(1 - \hat{p}_0 - \hat{n}(\hat{S}, \hat{t})), \tag{18}$$

implying that growth of the spheroid occurs purely through the absorption or leakage of

the cellular material and not directly by cell reproduction. The results of a simulation with  $\delta = \hat{\lambda} = 1$  are discussed in detail in the next section.

In the following sections the carets on the variables and parameters are dropped for brevity.

### 3. Numerical solution of the time-dependent problem

#### 3.1 Numerical methods

The system of equations (12)–(14) is too complex for analytical solution with general parameter values, and we therefore resort to the use of numerical methods. The aims are to assess whether the model captures qualitatively, and preferably quantitatively, all significant features of spheroid growth and to establish the range of parameter values which provides the most realistic behaviour. Finite-difference methods are used to approximate the solutions to the system (13)–(14) together with (17). The system of equations are rescaled using  $r = S(t)\rho$ , fixing the moving domain onto the unit interval and leading to the following system for numerical solution

$$\frac{\partial n}{\partial t} + \frac{v - \rho \dot{S}}{S} \frac{\partial n}{\partial \rho} = D_p \frac{n}{\rho^2 S^2} \frac{\partial}{\partial \rho} \left( \rho^2 \frac{\partial n}{\partial \rho} \right) + n[a(c, 1-n) - nb(c, 1-n)], \quad (19)$$

$$\frac{1}{\rho^2} \frac{\partial}{\partial \rho} \left( \rho^2 \frac{\partial c}{\partial \rho} \right) = S^2 k(c, 1-n)n, \quad (20)$$

$$\frac{1}{\rho^2} \frac{\partial(\rho^2 v)}{\partial \rho} = Sb(c, 1-n)n - \frac{1}{S} \frac{D_p}{\rho^2} \frac{\partial}{\partial \rho} \left( \rho^2 \frac{\partial n}{\partial \rho} \right). \quad (21)$$

The system of equations is solved sequentially by a predictor–corrector-type scheme. Equation (19) is solved first in conservation form using the NAG routine D03PGF, which uses the method of lines and a backward-differencing time step. Then equation (20) is solved using the NAG routine D02AGF, which uses a finite-difference approach together with Newton iteration. Second-order schemes to approximate (21) were found to be inadequate to provide sufficiently accurate solutions for D03PGF to converge efficiently. This difficulty was overcome by integrating (21) to give

$$v = \frac{S(t)}{\rho^2} \int_0^\rho \xi^2 b(c, 1-n)n \, d\xi - \frac{D_p}{S(t)} \frac{\partial n}{\partial \rho},$$

where the integral was evaluated by the trapezium method with correction and a five-point interpolation method was used for the derivative term, resulting in a fourth-order accurate approximation for  $v$ . Further details of this approximation for  $v$  is given in Ward (1997). Finally,  $S$  is evaluated using the trapezium method on  $dS/dt = v(S, t)$ . The system is solved on a mesh which is contracting towards  $\rho = 1$  in order to overcome the difficulty resulting from the boundary layer that forms at the surface as the spheroid size gets large; 200 or 500 mesh points are usually used.

3.2 Numerical results

With so little data concerning the nature of necrotic material available, the relevant parameters used in the simulations which follow are estimates, leading to reasonable quantitative results at growth saturation. The ‘standard’ set of values used for the dimensionless parameters which also occur in the model of Ward & King (1997) is

$$\left. \begin{aligned} B/A &= 0.5, & \sigma &= 0.9, \\ c_c &= 0.1, & c_d &= 0.1, & m_1 &= 1, & m_2 &= 1, \\ \beta_1 &= 0.01, & \beta_2 &= 0, & \delta &= 1, \end{aligned} \right\} \quad (22)$$

and the ‘standard’ set of values for the other dimensionless parameters is

$$\left. \begin{aligned} \lambda &= 1, \\ D_p &= 300, & Q_p &= 10, & p_0 &= 0.1, \\ p_c &= 0.1, & m_3 &= 1. \end{aligned} \right\} \quad (23)$$

Simulations resulting from varying one or more of these parameters are presented later in this section. The external cellular material concentration ( $p_0 = 0.1$ ) is thus fairly small and the choice  $\lambda = 1$  and  $\delta = 1$  implies there is no local volume change on cell death or mitosis and it suggests, with  $D_p$  being fairly large, that leakage will be the dominant mechanism for necrotic-volume loss. We note that the choice of  $\lambda = \delta = 1$  implies from equation (14) that the velocity field is driven only by the diffusion of the necrotic material, and equation (18) implies that the growth rate is governed by the material flux at the surface. The diffusion coefficient for the cellular material is discussed in Appendix A, and rescaling leads to  $D_p = 300$ , representing material with molecular mass of  $O(10^5)$ . The above choices of values for  $\beta_1$  and  $\beta_2$  imply that the consumption rate of the nutrient is independent of the concentration of cellular material.

The results of simulations using the above parameter values are illustrated in Figs. 1–4. We observe in Fig. 1 that, with these parameter values, the main phases of spheroid growth are all captured. Close inspection for early time reveals a short period of accelerating growth (the exponential phase), then retardation to a phase between about  $t = 20$  and  $t = 100$  in which growth appears linear and from which growth retardation continues towards the saturation state. This early-time behaviour is demonstrated in the analysis of Appendix B, which is based on that of Section 5 in Ward & King (1997) and involves a limiting case of the model in which the death rate,  $B/A = \varepsilon$ , is small and  $D_p, Q_p = O(1/\varepsilon)$ . In the case  $\beta = \beta_1 + \beta_2 \ll 1$  we then find that the initial growth of the spheroid is described by  $S \sim \exp[k_m(1, p_0)t/3]$ . Retardation first occurs on a time scale of  $t = O(\ln(1/\beta))$  due to quiescence in the core, leading to a phase of linear growth with  $S \sim qt$ , for some constant  $q$  given in Appendix B. The dashed curve indicates the growth in time of a measure of the size of the necrotic core, taken to be the radius at which the live-cell density has the value  $n = 0.1$ . Close inspection of this curve reveals that it expands at a faster rate than the spheroid surface, which is consistent with the experimental observations of Groebe & Mueller-Klieser (1996) and Tannock & Kopelyan (1986a). The evolution of the live-cell density towards the steady-state profile (solid curve) is depicted in Fig. 2; the steady-state profile is generated from the numerical solution of the appropriate system of equations derived in Section 4. Following an initial transient of cellular material influx from the exterior,

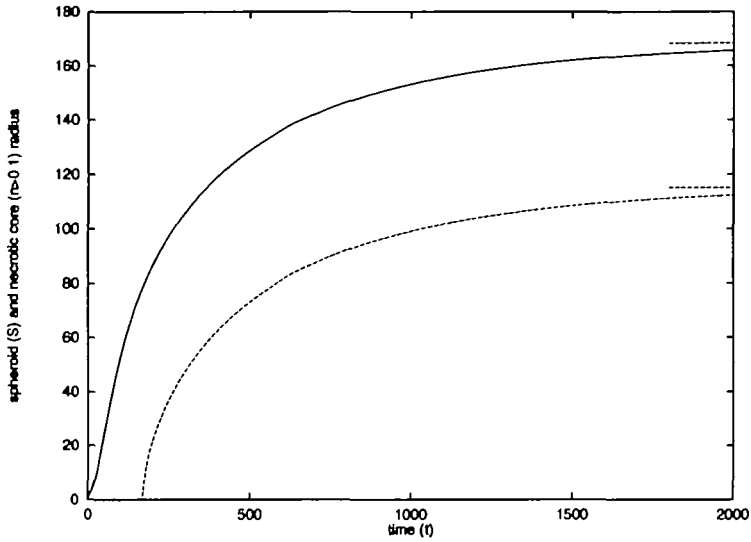


FIG. 1. (—) The dimensionless tumour radius and (---) necrotic core radius (defined to be where  $n = 0.1$ ) plotted against time. The two dashed lines to the right indicate the corresponding values at saturation.

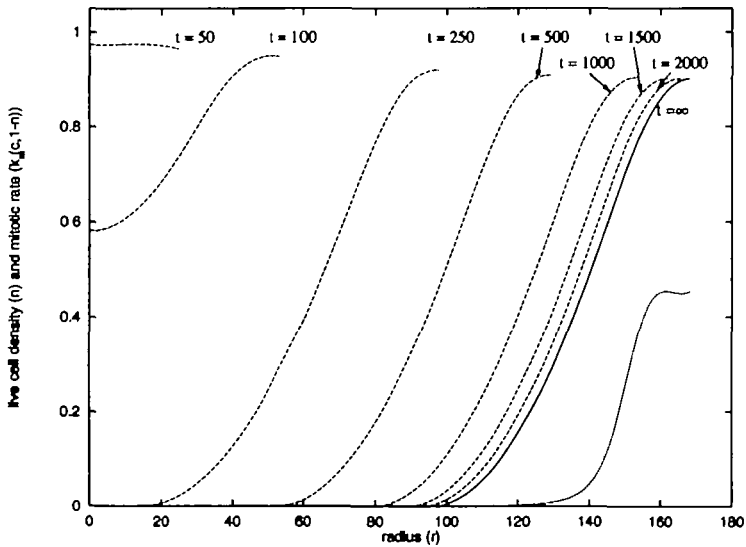


FIG. 2. Evolution of (---) the spatial distribution of live-cell density towards (—) the steady-state solution. (···) The distribution of the mitotic rate at the steady state.

the live-cell density during the early phases reaches a fairly constant level, the delivery of material by diffusion balancing its consumption during mitosis. As the spheroid gets larger and the central nutrient concentration declines in the core (see Fig. 3), cell death increases, so that by  $t = 250$  an almost completely necrotic core has developed. This profile is ap-

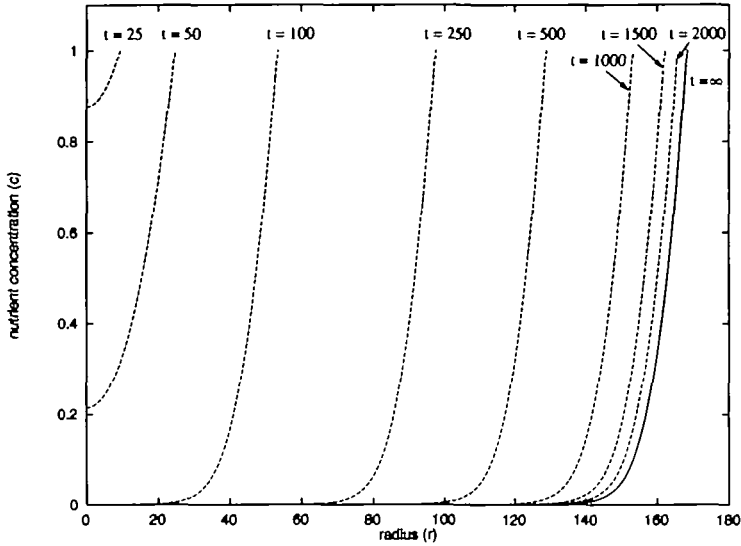


FIG. 3. Evolution of (---) the nutrient concentration towards (—) the steady-state solution.

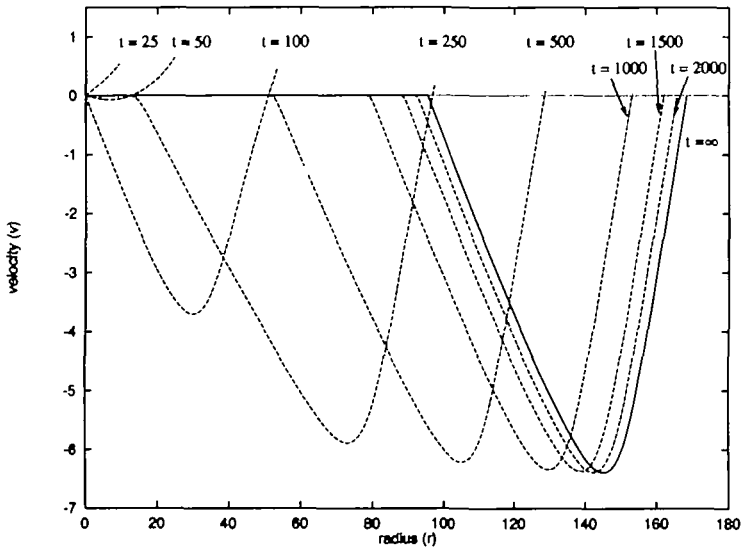


FIG. 4. Evolution of (---) the velocity distribution towards (—) the steady-state solution.

proximately maintained as it develops towards the steady state. We note that, at saturation, equation (18) implies that  $n(S_{\infty}, t) = 1 - p_0 = 0.9$ . The long time (steady-state) solutions for this case have a core region of complete necrosis (that is, with  $n \equiv 0$ ), there being an interface dividing a core of zero live-cell density from an outer rim of living cells: At this interface the second derivative is not continuous, and so these steady solutions are weak

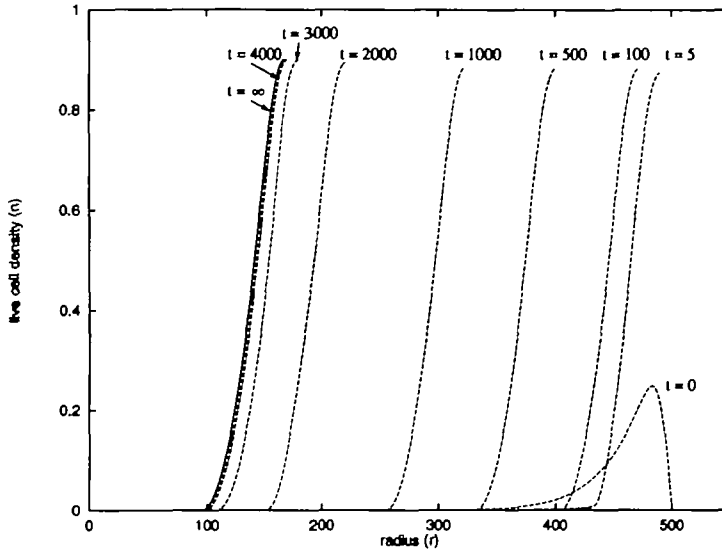


FIG. 5. Evolution of (---) the live-cell density towards (—) the steady-state solution for different initial conditions.

solutions to the model, live cells being conserved at the interface. The physical relevance of this type of solution is clear, representing complete necrosis in the core. The dotted curve in Fig. 2 shows the distribution of the mitotic rate at the steady state. The curve is observed to plateau in the outer rim, descending to zero as the nutrient concentration diminishes towards the core. The main feature of note is that the living cells just inside from the rim are quiescent, the mitotic rate there being at a very low level. Thus, the resulting saturated spheroid has the three-layered structure observed in multicell spheroids. In Fig. 3 we observe that the consumption of the nutrient by the living cells in the viable rim leads to a rapid descent in the nutrient concentration over this region. The fourth derivative of its steady state is discontinuous at the interface described above,  $c$  attaining a uniform value in the core. Figure 4 shows the development of the velocity distribution towards the steady-state solution (solid curve). In the early stages (see  $t = 25$ ) the influx of material from the surface dominates throughout the spheroid and the velocity is positive everywhere. As the spheroid gets larger and necrosis in the core becomes significant, the necrotic products seep into the rim causing flow in the opposite direction ( $t \geq 50$ ), leading to the kind of profiles observed in the simpler model of Ward & King (1997). We note that the first derivative of the steady-state velocity profile is discontinuous at the interface described above,  $v$  being identically zero in the core. As the spheroid approaches saturation, equation (18) implies that the flux at the surface equilibrates and seepage of material from the core balances its creation and consumption from cell death and mitosis.

In order to investigate whether the steady state is an attractor for very different initial conditions, Fig. 5 shows the evolution of the live-cell density using the same parameter set but with different, and artificial, initial conditions. In view of the initial distribution, the live-cell density rapidly rises in the rim due to the combination of cellular material

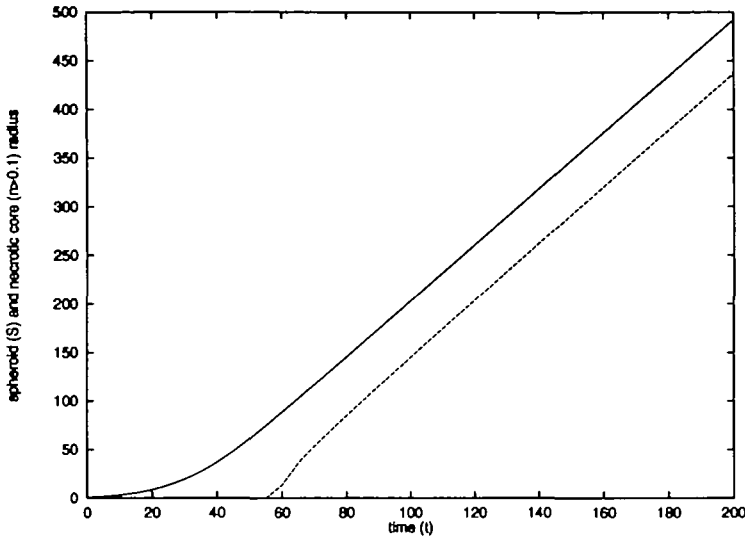


FIG. 6. (—) The spheroid radius and (---) the necrotic core radius (defined to be where  $n = 0.1$ ) plotted against time for a travelling-wave situation, with  $\lambda = 0.5$ .

absorption through the surface and mitosis, and by  $t = 5$  the familiar type of profile is restored, which then propagates back towards the steady state (the same as that shown in Fig. 2) as the necrotic core contracts, mainly due to the leakage of the excess necrotic material. However, the choice of the values of  $Q_p$  and  $D_p$ , with  $Q_p/D_p$  small, implies that the rate of leakage is small, causing the slow contraction. When leakage is significant, the value of  $Q_p/D_p$  is important in governing the speed at which the spheroid approaches the steady state. However, we note in this particular simulation, with  $\lambda = \delta = 1$ , (18) implies that at steady state the solutions are independent of the parameter  $Q_p$ . The steady-state solution shown in Fig. 5 is the only nontrivial long-time solution found using the numerical methods described in Section 5, and the results suggest it is a global attractor. In certain parameter regimes, however, two nontrivial long-time solutions exist; an example is given in a later figure.

In Figs. 6–8 the other main classes of solutions are illustrated by varying  $\lambda$ , with the other parameter values still given by (22) and (23). Setting  $\lambda = 0.5$  leads to solutions of travelling-wave type, and the growth curve is illustrated in Fig. 6 together with a measure of the necrotic core radius (again defined to be where  $n = 0.1$ ). Figure 6 demonstrates the expected acceleration of growth up to about  $t = 40$ , evolving ultimately to linear growth. As with the simpler model of Ward & King (1997), linear growth implies a rim of constant thickness of viable cells. In Fig. 7 we observe that during the linear growth phase the live-cell distribution maintains its profile whilst propagating outward. Unlike the solutions described above, the long-time solutions for  $n$  decay exponentially into the core, giving an important distinction between the travelling-wave and steady-state limits of the model. Close inspection of the live-cell distribution at the rim reveals that  $\partial n/\partial r > 0$  there, implying that leakage of the necrotic material from the spheroid is occurring; however, not enough necrotic volume is being lost or consumed during mitosis for growth to cease.

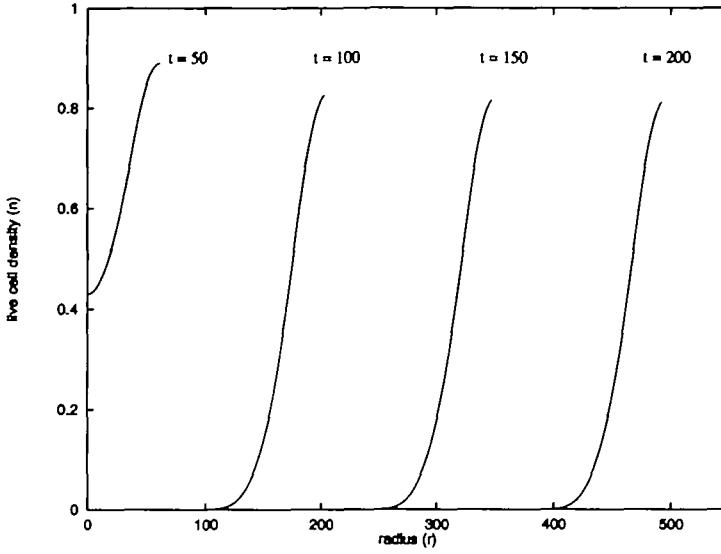


FIG. 7. Evolution of the live-cell-density distribution for a travelling-wave situation, with  $\lambda = 0.5$ .

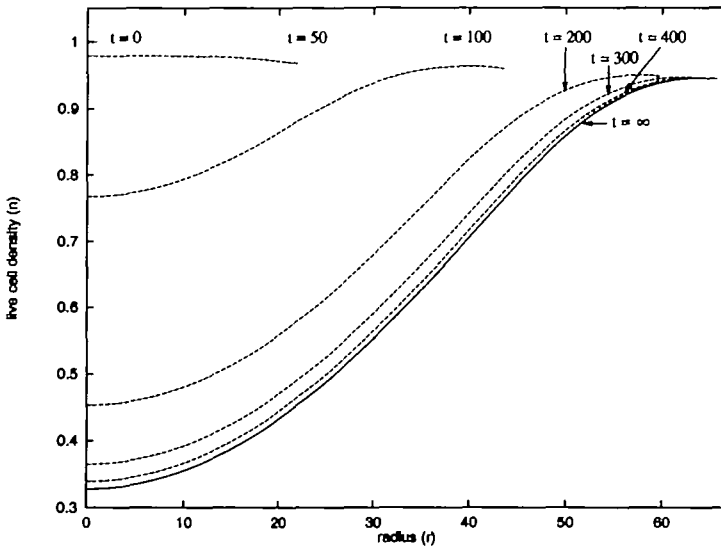


FIG. 8. Evolution of (---) the live-cell density towards (—) a steady-state solution with a partially necrotic core, with  $\lambda = 1.1$ .

The evolution of the live-cell distribution for the case of  $\lambda = 1.1$  is shown in Fig. 8. We observe that a steady-state is achieved (the solid curve); however, living cells still survive in the core, albeit in a quiescent state. It is not clear from Fig. 8, but it is easy to show from integrating (14) with  $\delta = 1$  and  $\lambda > 1$ , that  $\partial n / \partial r < 0$  at the rim, implying there is

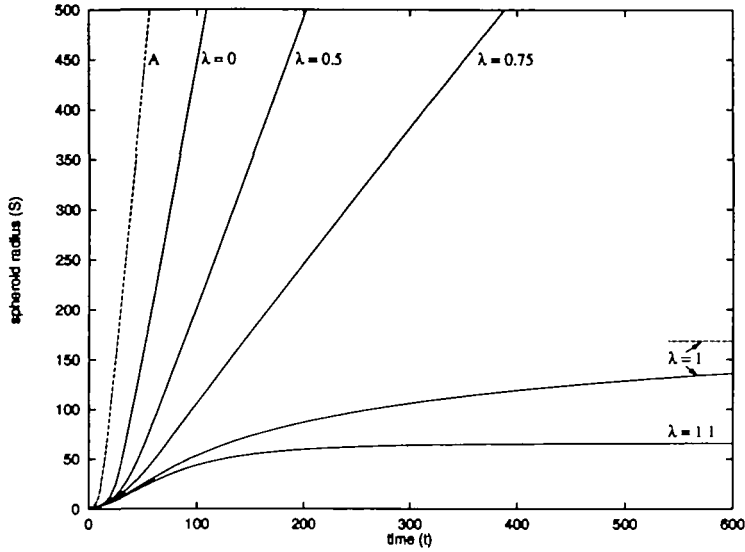


FIG. 9. Effects of the mitotic contraction factor,  $\lambda$ , on spheroid growth. The dashed curve labelled A is the solution of the simpler model of Ward & King (1997). The dashed line on the right indicates the final saturation size.

influx of material from external medium. However, the cellular material is consumed at a sufficiently high rate to cause growth saturation.

Figure 9 shows the spheroid radius against time for various values  $\lambda$ , with all the other parameters given by (22) and (23). Figure 9 shows that, below a threshold (in this case,  $\lambda \approx 0.86$ ), insufficient cellular material is utilized to cause saturation, resulting in travelling-wave behaviour. Above this threshold, increasing  $\lambda$  results in a spheroid of smaller saturation size. For  $\lambda = 0$ , the only necrotic-volume-loss mechanism is leakage and Fig. 9 demonstrates the retarding effect that this mechanism has in comparison with solution of the model of Ward & King (1997) (curve B), with the parameters also given by (22).

Figure 10 shows the evolution of the spheroid using the parameter set (22) and (23), except that  $D_p = Q_p = 250$ ,  $\lambda = 0.4$ , and  $p_0 = 0$ , indicating zero concentration of cellular material in the external matrix. Here, there are two possible long-time solutions, in addition to the trivial solution which corresponds to the tumour dying off. Both of these are steady states, one having a fully developed necrotic core (with saturation size  $S_\infty \approx 148.36$ ) and the other with a partially necrotic core (with  $S_\infty \approx 28.52$ ). In Fig. 10 the smaller of these steady states was used as the initial conditions (in terms of the rescaled variable  $\rho$ ) for curves A–C, except that in curves A and C the initial size of the spheroid was set to  $S(0) = 29.52$  and  $S(0) = 27.52$ , respectively. The divergence of curves A and C away from curve B demonstrates the instability of the smaller steady-state solution: curve A ultimately tends towards the larger steady state and curve C ultimately vanishes, implying that the spheroid dies off. This suggests that the trivial state is stable to sufficiently small perturbations, being an attractor for tumours of sufficiently small initial size. This is in contrast to all other simulations illustrated in this section. The stability of the trivial

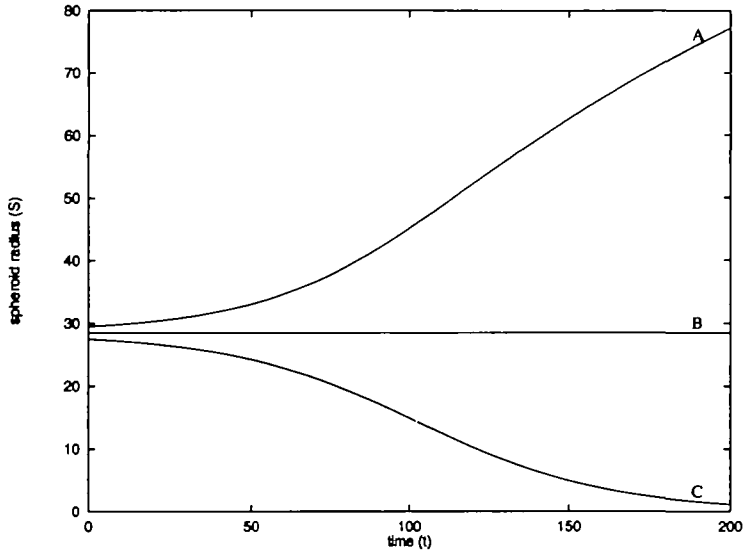


FIG. 10. The spheroid radius plotted against time for three initial sizes of spheroid: (A)  $S(0) \approx 29.52$ , (B)  $S(0) \approx 28.52$ , and (C)  $S(0) \approx 27.52$ .

state in this case is perhaps not surprising. With zero external concentration of cellular material, cells must die within the spheroid in order to generate the material to create new cells through mitosis. However, if there are only a few cells present the production of the material will be inadequate, making the spheroid unsustainable. In fact, it can be shown from the analysis of Section 5.3 that the trivial solution is stable for  $p_0 < 1/90$  using these parameters.

Figure 11 shows the effects of the diffusion coefficient  $D_p$  for the leakage-only model, where we have used data set (22) together with  $Q_p = 100$  and  $\lambda = p_c = p_0 = 0$ . Increasing the diffusion rate implies that there is greater seepage of necrotic products from the core into the rim, from where it subsequently leaks out of the spheroid. Consequently, for smaller values of  $D_p$  there is insufficient leakage to cause saturation, and the travelling-wave solution results for long time, this being illustrated. The bifurcation between the travelling-wave and steady-state solutions can be determined from the formulations of Section 4 and occurs at  $D_p \approx 897$  in this case. Growth in the early phases is similar up to about  $t = 15$ , when necrosis begins and the diffusion and leakage of the necrotic products results in the divergence of the curves.

#### 4. Large-time behaviour: Formulation

##### 4.1 Introduction

The numerical solutions presented in Section 3 revealed that, depending on the values of the parameters, growth will ultimately tend either to a linear rate or saturate to a steady-state size. In this section both the travelling-wave and steady-state limits are investigated, and the bifurcation between the two outcomes is discussed.

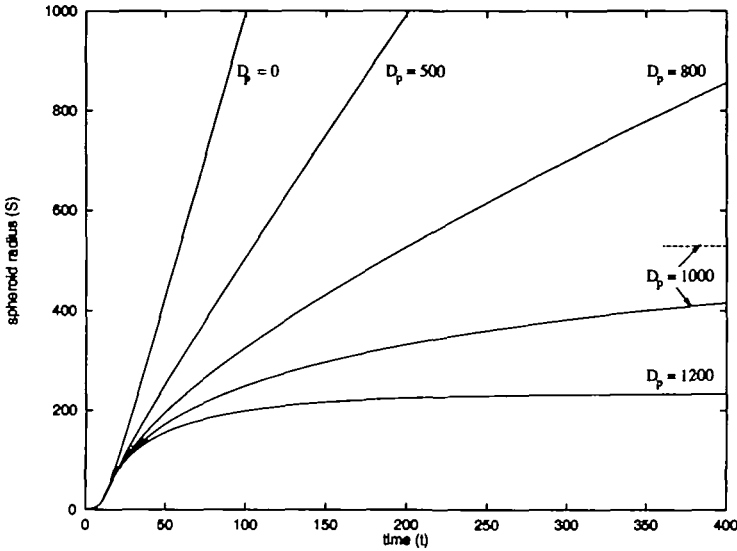


FIG. 11. Effects of the cellular material diffusion coefficient,  $D_p$ , on spheroid growth in the leakage-only model. The dashed line on the right indicates the final saturation size.

4.2 Travelling-wave solutions

Here we assume that the rate of spheroid growth tends towards an as yet undetermined constant speed  $U > 0$ , so that  $S \sim Ut$  as  $t \rightarrow \infty$ . We translate to travelling-wave coordinates using  $z = r - S(t)$ , with  $z < 0$ , obtaining the following system of ordinary differential equations:

$$D_p n n'' = (v - U)n' - n(a - bn), \tag{24}$$

$$c'' = kn, \tag{25}$$

$$v' = bn - D_p n'', \tag{26}$$

where the primes denote  $d/dz$ ; we note that the  $r^{-1} \partial/\partial r$  terms are  $O(S^{-1})$  as  $S \rightarrow \infty$  and are therefore neglected in the limit  $t \rightarrow \infty$ . The boundary conditions for the travelling-wave system are

$$\begin{aligned} n'(-\infty) = c'(-\infty) = v(-\infty) = 0, \\ D_p n'(0) = -Q_p(1 - p_0 - n(0)), \quad c(0) = 1, \quad v(0) = U. \end{aligned} \tag{27}$$

The system (24)–(26) is fifth order with six boundary conditions, which are apparently sufficient to determine the five variables  $n$ ,  $n'$ ,  $c$ ,  $c'$ , and  $v$ , and the remaining unknown  $U$ . We are not aware of any rigorous work to confirm such a statement, or of equivalent results for the steady-state systems below; however, the numerical work outlined below suggests that these systems are indeed well posed.

It can be shown using a far-field analysis that as  $z \rightarrow -\infty$  we have  $n \rightarrow 0$  and  $c \rightarrow C_0$  (constant); linearizing about these values yields

$$U n' \sim -a(C_0, 1)n, \tag{28}$$

implying exponential decay as  $z \rightarrow -\infty$  (we note that  $a(C_0, 1) < 0$  is thus required). This feature of exponential decay distinguishes solutions of the travelling-wave problem from steady states, which may contain a core of  $n \equiv 0$ ; we note that the linearization leading to (28) fails when  $U = 0$ .

As an aside, we can use the fact that  $n$  vanishes as  $z \rightarrow -\infty$  to reduce the system of equations (24)–(26) by one in the special case  $\beta_1 = 0$  (so that  $k(c, 1-n) = \beta_2 k_m(c, 1-n)$ ). Noting that  $[(v-U)n]' = (k_m - k_d)n$ , the substitution of this and equation (25) into (26) yields on integration

$$v = \frac{1}{1 - (1 - \delta)n} \left( \frac{\delta - \lambda}{\beta_2} c' - (1 - \delta)nU - D_p n' \right), \quad (29)$$

using  $n(-\infty) = 0$  together with  $n'(-\infty) = c'(-\infty) = v(-\infty) = 0$ . To eliminate  $v$  from the resulting system we use  $v(0) = U$  to get the boundary condition

$$U = \frac{\delta - \lambda}{\beta_2} c'(0) - Q_p(1 - p_0 - n(0)),$$

where we have used  $D_p n'(0) = Q_p(1 - p_0 - n(0))$ .

### 4.3 Steady-state solutions

In the usual way, we assume here that the  $\partial/\partial t$  terms vanish as  $t \rightarrow \infty$ . By assumption, the spheroid is ultimately of finite size. The steady-state system is

$$n \frac{D_p}{r^2} \frac{d}{dr} \left( r^2 \frac{dn}{dr} \right) = v \frac{dn}{dr} - n(a - bn), \quad (30)$$

$$\frac{1}{r^2} \frac{d}{dr} \left( r^2 \frac{dc}{dr} \right) = kn, \quad (31)$$

$$\frac{1}{r^2} \frac{d}{dr} \left( r^2 v \right) = bn - \frac{D_p}{r^2} \frac{d}{dr} \left( r^2 \frac{dn}{dr} \right), \quad (32)$$

which hold for  $0 < r < S_\infty$ , where  $S_\infty$  is the (unknown) saturation size of the spheroid and is therefore the coordinate of a free boundary.

As mentioned above, the degeneracy of the effective diffusion coefficient in the equation for  $n$ , (30), gives rise to the possibility of steady-state solutions that have a fully necrotic core (a region where  $n \equiv 0$ ), as well as smooth solutions with a partially developed necrotic core ( $n(0) > 0$ ). Thus the appropriate boundary conditions are dependent on the type of steady-state solution sought, and are listed below.

(i) *Partially necrotic core solutions.* The boundary conditions are

$$\begin{aligned} n'(0) &= c'(0) = v(0) = 0, \\ D_p n'(S_\infty) &= Q_p(1 - p_0 - n(S_\infty)), \quad c(S_\infty) = 1, \quad v(S_\infty) = 0, \end{aligned} \quad (33)$$

where the primes now denote  $d/dr$ . These six boundary conditions are sufficient to determine the five variables ( $n$ ,  $n'$ ,  $c$ ,  $c'$  and  $v$ ) and the coordinate of the free boundary  $S_\infty$ .

(ii) *Fully necrotic core solutions.* For this type of solution, there is a further free boundary at  $r = R_\infty$ , say, such that for  $r < R_\infty$  we have  $n \equiv 0, v \equiv 0$ , and  $c \equiv C_0 \geq 0$  (an unknown constant), and the system (30)–(32) applies in the region  $R_\infty < r < S_\infty$ , with the boundary conditions

$$\begin{aligned} n(R_\infty) = n'(R_\infty) = c'(R_\infty) = v(R_\infty) = 0, \\ D_p n'(S_\infty) = Q_p(1 - p_0 - n(S_\infty)), \quad c(S_\infty) = 1, \quad v(S_\infty) = 0. \end{aligned} \tag{34}$$

In this problem there are seven boundary conditions to determine the five variables ( $n, n', c, c'$  and  $v$ ) in  $R_\infty < r < S_\infty$ , leaving two conditions to determine the two free boundaries  $R_\infty$  and  $S_\infty$ . It should be stressed, however, that the solution to the time-dependent problem does not have a fully necrotic core, the behaviour in the limit  $t \rightarrow \infty$  being nonuniform. Linearized analysis on the time-dependent model reveals that the live-cell density in the core decays exponentially, satisfying  $\partial n / \partial t \sim a(c|_{t=\infty}, 1)n$  as  $t \rightarrow \infty$ , where  $c \sim c|_{t=\infty} = c(R_\infty)$ , with equation (15) implying that  $a(c|_{t=\infty}, 1) < 0$ .

The bifurcation between these two types of steady-state solution occurs when  $n(0)$  reaches zero in the partially necrotic formulation or  $R_\infty$  drops to zero in fully necrotic case. This special case has the following boundary conditions at  $r = 0$ :

$$n(0) = n'(0) = c'(0) = v(0) = 0, \tag{35}$$

plus the three conditions imposed at  $r = S_\infty$ . There are seven boundary conditions to determine the five variables ( $n, n', c, c'$ , and  $v$ ) and the free boundary  $S_\infty$ , leaving the problem overspecified, as required since a relation between the parameters must hold for the steady-state solution to lie on a bifurcation point between fully and partially necrotic core solutions.

As with the travelling-wave equations, the order of the steady-state system can be reduced by one when  $\beta_1 = 0$ , so  $k(c, 1 - n) = \beta_2 k_m(c, 1 - n)$ . Substituting  $r^{-2}d(r^2vn)/dr = (k_m - k_d)n$  and (31) into (32) eventually gives

$$v = \frac{1}{1 - (1 - \delta)n} \left( \frac{\delta - \lambda}{\beta_2} \frac{dc}{dr} - D_p \frac{dn}{dr} \right), \tag{36}$$

using  $v(0) = dn(0)/dr = dc(0)/dr = 0$ . We can eliminate  $v$  using  $v(S_\infty) = 0$  to obtain at  $r = S_\infty$ :

$$\frac{\delta - \lambda}{\beta_2} \frac{dc}{dr} = Q_p(1 - p_0 - n).$$

If we let  $r = \rho S_\infty$ , then, for large  $S_\infty$ , it can easily be shown that outer solutions (which hold for  $\rho = O(1)$  with  $\rho < 1$ ) take the form  $n \equiv 0, v \equiv 0, c \equiv c_0$ , for constant  $c_0$ , to all powers of  $1/S_\infty$ . This suggest that for large spheroids the steady-state solutions is fully necrotic in the core, the solution being nontrivial only in a boundary layer region  $1 - \rho = O(S_\infty^{-1})$ . There exists a smooth transition from the travelling-wave speed limit  $U \rightarrow 0$  to the steady-state limit of saturation size  $S_\infty \rightarrow \infty$ . This is exploited below to derive the equations for the travelling-wave/steady-state bifurcation. It is possible to show that at such a bifurcation point we have  $dS/dt \sim \gamma/S$  as  $t \rightarrow \infty$ , for some constant  $\gamma$ , giving sublinear growth,  $S \sim (2\gamma t)^{1/2}$ . Such behaviour has been confirmed numerically.

#### 4.4 The travelling-wave/steady-state bifurcation

This bifurcation is analysed by seeking steady-state solutions in the limit of  $S_\infty \rightarrow \infty$ . As stated above, the solutions for  $n$  and  $v$  in this limit are expected to be fully necrotic and we focus on the viable rim by translating the steady-state system (30)–(32), using  $x = r - S_\infty$ , to obtain at leading order as  $S_\infty \rightarrow \infty$

$$D_p n n'' = v n' - n(a - bn), \quad (37)$$

$$c'' = kn, \quad (38)$$

$$v' = bn - D_p n'', \quad (39)$$

the  $r^{-1}d/dr$  terms being of  $O(S_\infty^{-1})$  and therefore again being neglected. Defining  $x = X < 0$  to be the free-boundary coordinate of the unknown necrotic interface, so that for  $x < X$  we have  $n \equiv 0$ ,  $v \equiv 0$ , and  $c \equiv C_0$  (a constant), and for  $x > X$  we have (37)–(39) subject to

$$\begin{aligned} n(X) = n'(X) = c'(X) = v(X) = 0, \\ D_p n'(0) = Q_p(1 - p_0 - n(0)), \quad c(0) = 1, \quad v(0) = 0. \end{aligned} \quad (40)$$

We thus have seven boundary conditions to determine the five variables ( $n$ ,  $n'$ ,  $c$ ,  $c'$ , and  $v$ ) and the free boundary  $X$ ; this problem is again being overspecified, requiring some relation between the parameters to hold, thereby identifying the location of the bifurcation in parameter space.

#### 4.5 The consumption-only model

We now consider a special case in which substantially more progress can be made in characterizing the behaviour by analytical means. Here, we investigate the conditions for the existence of the long-time solutions for the consumption-only version of the model (that is, the case  $Q_p = 0$ ). The results below also apply to the zero diffusion case  $D_p = 0$ , where the problem reduces to the model of Ward & King (1997) generalized to include necrotic material consumption (if  $\lambda > 0$ ). Again defining  $z = r - Ut$ , then as  $t \rightarrow \infty$  the equations

$$[(v - U)n]' = (k_m - k_d)n, \quad (41)$$

$$v' = [(1 - \lambda)k_m - (1 - \delta)k_d]n - D_p n'', \quad (42)$$

hold for the travelling-wave case, where the primes denote  $d/dz$ , and the boundary values are  $v(0) = U$ ,  $v(-\infty) = 0$ . Substituting (41) into (42) yields

$$(1 - \delta)[(v - U)n]' = v' - (\delta - \lambda)k_m n + D_p n'',$$

which upon integration gives

$$U = (\delta - \lambda) \int_{-\infty}^0 k_m n \, dz, \quad (43)$$

since  $Q_p = 0$  implies that  $n'(0) = 0$ . Since  $U$  is required to be positive, and because the integral term on the right-hand side contains only positive quantities, we deduce that

$$\lambda < \delta \quad (44)$$

is a necessary condition for the existence of travelling-wave solutions for the consumption-only model.

It can easily be shown by repeating the above analysis on the steady-state equations that no nontrivial solutions exist for  $\lambda > \delta$ . Here, more cellular material is consumed during cell birth than produced at cell death, the tumour is unsustainable and eventually dies out. In the case  $\lambda = \delta$ , the steady-state system is underspecified and there are an infinite number of solutions parametrized by the saturation size  $S_\infty$ , the initial conditions determining the saturation size. The travelling-wave/steady-state bifurcation curve for the consumption only model is simply the line  $\lambda = \delta$ , on which this infinity of steady states lies.

**5. Large-time behaviour: Numerical solutions**

5.1 *Numerical methods*

The nonlinear nature of the above systems means that, except in special cases, we must again resort to numerical methods of solution. The governing problems either are, or will be reformulated as, two-point boundary-value problems, and a shooting method (NAG routine D02AGF) is used to solve each system. Improved convergence was gained by shooting from both sides and matching within the domain. A continuation procedure is incorporated, whereby an appropriate parameter adjusted, in order to track along the paths in parameter space, subsequent steps being linearly extrapolated from up to 15 of the previous steps.

5.2 *Formulation*

5.2.1 *Travelling-wave solutions* The travelling-wave system is reduced to a two-point boundary-value problem using the linearized solutions as  $z \rightarrow -\infty$  to provide asymptotic representations of the variables at a point  $z = -L$  for a suitably large value of  $L > 0$ . Rescaling equations (24)–(26) using  $y = z/L + 1$  and, defining  $\Upsilon = dn/dz$  and  $\Psi = dc/dz$ , the system can be restated as

$$n' = L\Upsilon, \tag{45}$$

$$\Upsilon' = L \left( \frac{(v - U)\Upsilon}{D_p} \frac{\Upsilon}{n} - \frac{a - bn}{D_p} \right), \tag{46}$$

$$c' = L\Psi, \tag{47}$$

$$\Psi' = Lkn, \tag{48}$$

$$v' = L \left( a - (v - U) \frac{\Upsilon}{n} \right), \tag{49}$$

where the primes now denote d/dy. Using the linearized approximations at  $z = -L$  the following set of boundary conditions is imposed

$$\text{at } y = 0 \quad n = \mathcal{N}_0, \quad \Upsilon = -a\mathcal{N}_0/U, \quad c = C_0 + (U/a)^2 k\mathcal{N}_0,$$

$$\Psi = -(U/a)k\mathcal{N}_0, \quad v = (D_p a^2 - bU^2)\mathcal{N}_0/aU,$$

$$\text{at } y = 1 \quad n = N_1, \quad \Upsilon = Q_p(1 - p_0 - N_1)/D_p, \quad c = 1, \quad v = U,$$

where  $\mathcal{N}_0 = N_0 \exp(aL/U)$ ,  $N_0$  being an arbitrary constant of integration arising from the linearized analysis and  $a$  denotes  $a(C_0, 1)$  (and similarly for  $b$  and  $k$ ). Here,  $N_0$ ,  $C_0$ , and  $N_1$ , as well as  $U$ , are determined as part of the solution; thus, fixing  $L$ , we have a fifth-order system and four unknown parameters with nine boundary conditions, indicating the problem to be correctly specified.

**5.2.2 Steady-state solutions** The domain on which the system (30)–(32) is to be approximated depends on the type of solution. In the partially necrotic core case the system is integrated over the whole spheroid, whilst in the fully necrotic core case we integrate between the two free boundaries  $R_\infty$  and  $S_\infty$ . These two cases and their bifurcation are therefore discussed separately.

(i) *Partially necrotic core.* The presence of the terms in  $r^{-1}$  in this case causes numerical problems as  $r \rightarrow 0$ ; these are tackled by introducing approximate boundary conditions at a point  $r = \epsilon$ , with  $\epsilon \ll 1$ , which are derived from a power series solution of the system (30)–(32) as  $\epsilon \rightarrow 0$ . In order to solve on the unit interval we define  $y = (r - \epsilon)/L$ , where  $L = S_\infty - \epsilon$ , and write  $\Upsilon = dn/dr$  and  $\Psi = dc/dr$ . The system can then be restated as

$$n' = L\Upsilon, \tag{50}$$

$$\Upsilon' = -\frac{2L}{y}\Upsilon + L\left(\frac{v\Upsilon}{D_p n} - \frac{a - bn}{D_p}\right), \tag{51}$$

$$c' = L\Psi, \tag{52}$$

$$\Psi' = -\frac{2L}{y}\Psi + Lkn, \tag{53}$$

$$v' = -\frac{2L}{y}v + L\left(a - \frac{v\Upsilon}{n}\right), \tag{54}$$

where the primes again denote  $d/dy$ , with  $\mathcal{Y} = yL + \epsilon$ , and equation (51) is used in obtaining (54). The boundary values used employ the first correction terms in the series expansion, and for fixed  $\epsilon \ll 1$  they are

$$\begin{aligned} \text{at } y = 0 \quad n &= N_0 + \epsilon^2 \mathcal{N}_1, \quad \Upsilon = 2\epsilon \mathcal{N}_1, \quad c = C_0 + \epsilon^2 C_1, \\ &\quad \Psi = 2\epsilon C_1, \quad v = \epsilon \mathcal{V}_1, \\ \text{at } y = 1 \quad n &= N_1, \quad \Upsilon = Q_p(1 - p_0 - N_1)/D_p, \quad c = 1, \quad v = 0, \end{aligned}$$

where

$$\begin{aligned} \mathcal{N}_1 &= -\frac{1}{6D_p} [a(C_0, 1 - N_0) - N_0 b(C_0, 1 - N_0)], \\ C_1 &= \frac{k(C_0, 1 - N_0)}{6} N_0, \\ \mathcal{V}_1 &= \frac{b(C_0, 1 - N_0)}{3} N_0 - 2D_p \mathcal{N}_1. \end{aligned}$$

Further terms in the series expansion can easily be found; however, for small enough  $\epsilon$  the above suffice. We require  $N_0$ ,  $C_0$ , and  $N_1$ , as well as  $S_\infty$ , to be determined and, by the usual arguments, this problem is expected to be correctly specified.

(ii) *Fully necrotic core.* In this case, the presence of the  $1/n$  term due to the nonlinearity of the live-cell ‘diffusion’ (see equation (51) above) causes numerical problems as  $r \rightarrow R_{\infty}^+$ . This is overcome, in similar fashion to above, by introducing an approximate boundary condition at a point  $r = R_{\infty} + \epsilon$  with  $0 < \epsilon \ll 1$ , again using power-series expansions to give the local behaviour of the variables. In order to solve on the unit interval, we fix  $\epsilon$  and define  $y = (r - R_{\infty} - \epsilon)/L$ , where  $L = S_{\infty} - R_{\infty} - \epsilon$ ; defining  $\Upsilon$  and  $\Psi$  as before we recover the system (50)–(54) with  $\mathcal{Y} = yL + R_{\infty} + \epsilon$ . Using the small  $\epsilon$  results at  $y = 0$  yields the boundary conditions

$$\begin{aligned} \text{at } y = 0 \quad n &= \epsilon^2 \mathcal{N}_2, \quad \Upsilon = 2\epsilon \mathcal{N}_2, \quad c = C_0 + \epsilon^4 k(C_0, 1)\mathcal{N}_2/12, \\ \Psi &= \epsilon^3 k(C_0, 1)\mathcal{N}_2/3, \quad v = \epsilon a(C_0, 1)/3, \end{aligned} \tag{55}$$

$$\text{at } y = 1 \quad n = N_1, \quad \Upsilon = Q_p(1 - p_0 - N_1)/D_p, \quad c = 1, \quad v = 0,$$

where  $\mathcal{N}_2 = -a(C_0, 1)/6D_p$ . We therefore have as undetermined constants  $S_{\infty}$ ,  $R_{\infty}$ ,  $C_0$ , and  $N_1$  and believe the problem to be correctly specified.

(iii) *Partially/fully necrotic core bifurcation.* This case is the limits  $N_0 \rightarrow 0$  and  $R_{\infty} \rightarrow 0$  of, respectively, the partially and fully necrotic core cases. Here the  $1/n$  and  $1/r$  terms both cause problems as  $r \rightarrow 0$ . We take  $r = \epsilon$  as our left-hand point and rescale to the unit interval using  $y = (r - \epsilon)/L$ , where  $L = S_{\infty} - \epsilon$ , which leads to the system (50)–(54) with  $\mathcal{Y} = yL + \epsilon$ . However, since we are taking an expansion about  $r = 0$  the effects of the spherical geometry is non-negligible, and to the first correction term the boundary conditions are now

$$\begin{aligned} \text{at } y = 0 \quad n &= 3\epsilon^2 \mathcal{N}_2/5, \quad \Upsilon = 6\epsilon \mathcal{N}_2/5, \quad c = C_0 + \epsilon^4 k(C_0, 1)\mathcal{N}_2/20, \\ \Psi &= \epsilon^3 k(C_0, 1)\mathcal{N}_2/5, \quad v = \epsilon a(C_0, 1)/5, \end{aligned}$$

$$\text{at } y = 1 \quad n = N_1, \quad \Upsilon = Q_p(1 - p_0 - N_1)/D_p, \quad c = 1, \quad v = 0,$$

where  $\mathcal{N}_2 = -a(C_0, 1)/6D_p$ . The constants  $C_0$ ,  $N_1$ , and  $S_{\infty}$  need to be determined and, additionally, some relation must hold between the parameters in order to be at a bifurcation point.

**5.2.3 The travelling-wave/steady-state bifurcation** In this case we seek solutions to the system (37)–(39) over the region  $X < x < 0$ . However, the presence of the  $1/n$  term again prompts us to use a series expansions of the variables as  $x \rightarrow X^+$ . For small  $\epsilon$ , we take the starting point to be  $x = X + \epsilon$  and let  $L = -X - \epsilon$ , the domain being rescaled to the unit interval by defining  $y = 1 + x/L$ . The appropriate system for this bifurcation problem is the same as for the travelling-wave system (45)–(49) but with  $U = 0$ . The boundary conditions for this case are given by (55). The constants  $C_0$ ,  $N_1$ , and  $X$  must be determined as part of the solution, as must the relationship between the parameters which gives the bifurcation curve.

**5.3 Numerical results**

With so many parameters in the model, it is impractical to give an exhaustive survey of the effects of each of them on the long-time solution. Hence, for most of the results to follow

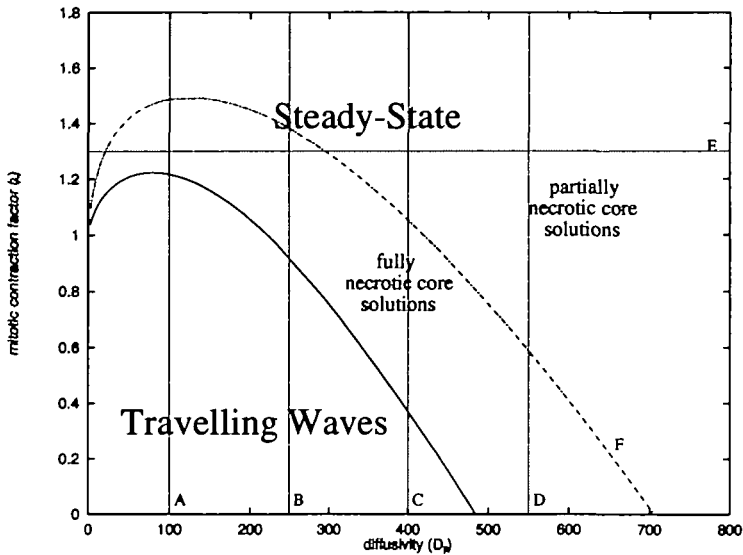


FIG. 12. The distribution of steady-state and travelling-wave solutions in  $(D_p, \lambda)$ -parameter space, showing (—) the travelling-wave/steady-state and (- · -) the fully/partially necrotic core bifurcations. The paths for Figs. 13–16 are indicated by the dotted lines labelled A–D and by dash-dot curve F.

the parameters that are shared with the model of Ward & King (1997) are kept fixed, being given by parameter set (22), while the new parameters are varied. In particular we shall focus on the travelling-wave growth velocity or the saturation size (as appropriate) and on the bifurcations between travelling-wave and steady-state solutions and between the fully and partially necrotic core solutions. Except where otherwise stated, we shall reduce the number of parameters to be studied by taking  $D_p = Q_p$  throughout what follows; the ratio  $D_p/Q_p$  determines the leakage rate and we are thus fixing leakage properties while varying other parameters.

The first of the bifurcation diagrams is shown in Fig. 12, where the regions of existence of the travelling-wave and steady-state solutions are shown in  $(D_p = Q_p, \lambda)$ -space, with all parameters other than  $D_p = Q_p$  and  $\lambda$  given by (22) and (23). We note that, with this data set, only a single nontrivial long-time solution with positive radius exists at any point in parameter space. The bifurcation curves were generated by tracking along the various branches, solving the bifurcation equations derived above. The solid curve marks the bifurcation between travelling-wave and steady-state solutions, and the dash-dot curve marks the bifurcation between fully and partially necrotic core solutions. Below the solid curve the combination of mitotic contraction and leakage is inadequate to cause cessation of growth, and travelling-wave solutions result. Above the solid curve lies a band consisting of fully necrotic core solutions, and the remainder of the quarter space consists of steady-state solutions with partially necrotic cores. In the latter region the effects of the combination of mitotic contraction and leakage are sufficiently strong that the resulting spheroid lacks a fully developed necrotic core. Both bifurcation curves are unimodal, and to the right of the maximum reach  $\lambda = 0$  at some finite  $D_p$ ; this is to be expected, since de-

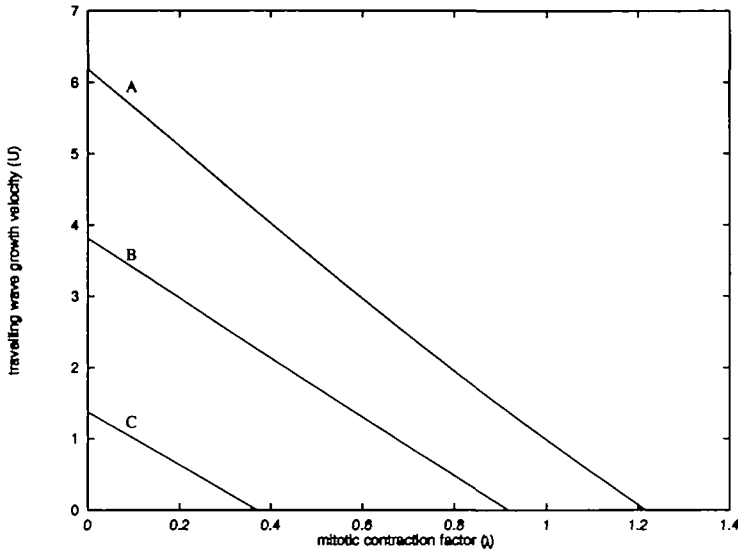


FIG. 13. Plots of travelling-wave growth speed against  $\lambda$  for three fixed values of  $D_p$ : (A) 100, (B) 250, and (C) 400.

creasing the mitotic contraction along the bifurcation curve requires an increase in amount of leakage in order to compensate. The decrease in  $\lambda$  as  $D_p$  decreases to the left of the maximum results from diffusion being so weak that the living cells depend more on the death of cells than on the external source to provide the cellular material necessary to reproduce; consequently to balance the usage and generation of cellular material the bifurcation curves descends towards  $\delta = \lambda = 1$ , as predicted by the analysis of Section 4.5.

The travelling-wave growth velocities and the saturated spheroid radii along the paths A–F in Fig. 12 are shown in Figs. 13–15. The growth velocities along paths A, B, and C, corresponding to values of  $D_p$  of 100, 250, and 400, respectively, are shown in Fig. 13. We note that the growth velocities descend approximately linearly towards zero at the travelling-wave/steady-state bifurcation point, with only line A showing any noticeable curve. Figure 14 shows the saturation spheroid size,  $S_\infty$ , as a function of  $\lambda$  for the paths labelled A–D. The dotted vertical lines show, from left to right, the positions of the travelling-wave/steady-state bifurcations for curves C–A. We observe in all cases an initial rapid decrease in  $S_\infty$  as  $\lambda$  increases, with a subsequent levelling following the fully/partially necrotic core bifurcation (indicated by the  $\diamond$  on each of the curves). The sensitivity of the  $S_\infty$  to  $\lambda$  over the region of fully necrotic solutions is noteworthy, though the influence of other factors not included in the model may mitigate this feature. Although not physically realistic, it can be shown by taking a regular expansion in the limit  $\lambda \rightarrow \infty$  that, provided  $n_0 + p_0 - 1 > 0$ , we have

$$S_\infty \sim \frac{Q_p}{\lambda} \frac{3(n_0 + p_0 - 1)}{n_0 k_m (1, 1 - n_0)}, \tag{56}$$

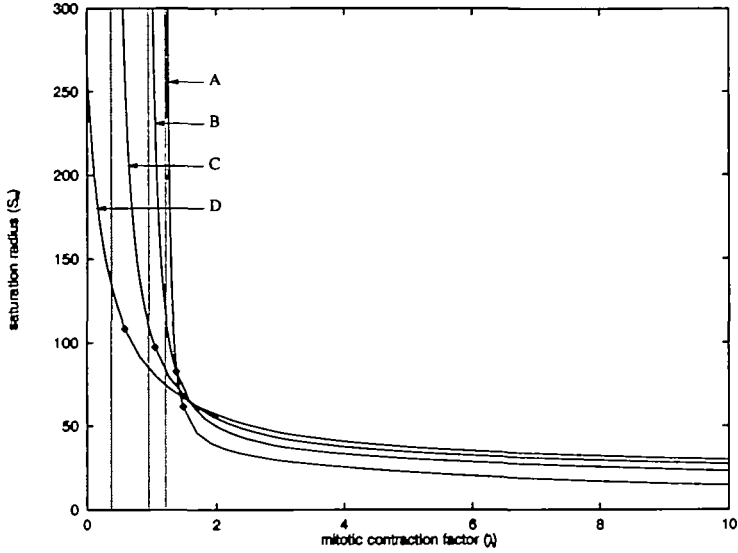


FIG. 14 Plots of saturated spheroid size against  $\lambda$  for four fixed values of  $D_p$ : (A) 100, (B) 250, (C) 400, and (D) 550. (o) The fully/partially necrotic core bifurcation points.

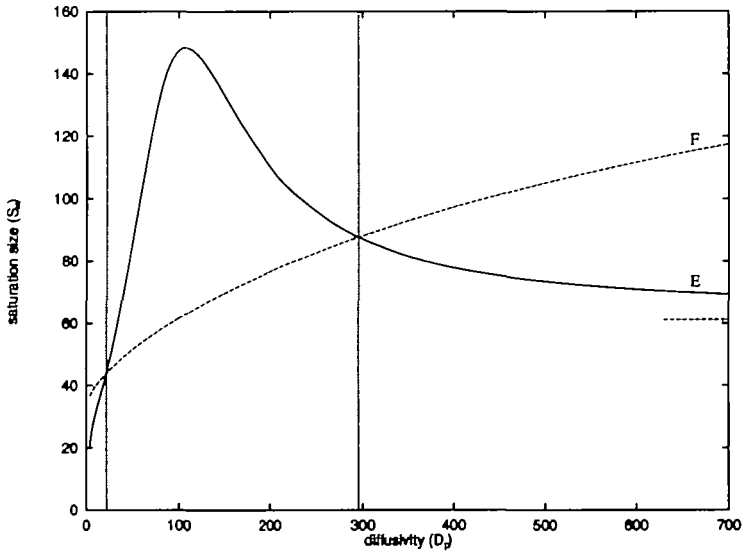


FIG. 15. Plots of (E) saturated spheroid size against  $D_p$  for  $\lambda = 1.3$  and (F) along the fully/partially necrotic core bifurcation. The dashed horizontal line on the right indicates the limit of curve E as  $D_p \rightarrow \infty$ . The two dotted vertical lines mark the boundaries of the fully necrotic core solutions.

where  $n_0$  is the solution of  $k_m(1 - n_0) = k_d(1)$ , so that

$$n_0 = 1 - p_c^{m_3} \left( \frac{k_d(1)(1 + c_c^{m_1})}{1 - k_d(1)(1 + c_c^{m_1})} \right)^{\frac{1}{m_3}} \tag{57}$$

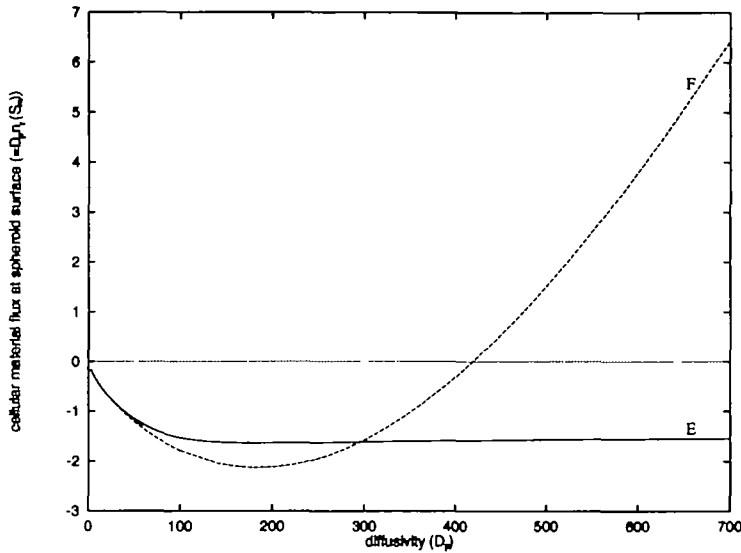


FIG. 16. Plots of cellular material flux at (E) the spheroid surface against  $D_p = Q_p$  for  $\lambda = 1.3$  and (F) along the fully/partially necrotic core bifurcation.

We note that for  $p_0 < 1 - n_0$ , equation (56) predicts a value of  $S_\infty$  that is negative, and the asymptotic expansion breaks down; however, it does reveal that  $p_0 = 1 - n_0$  marks a bifurcation of the long-time solutions between unique nontrivial solutions existing over the whole of the quarter space and two nontrivial solutions existing over part of the quarter space. An example of the latter case is described later.

The saturation size and surface flux of cellular material along path E ( $\lambda = 1.3$ ) and along the fully/partially necrotic core bifurcation F are shown in Figs. 15 and 16. The dotted vertical lines in Fig. 15 show the boundaries of the fully necrotic core solution region for curve E. Consistent with the result shown in Fig. 14,  $S_\infty$  reaches a peak within the fully necrotic core region, showing that the larger spheroids tend to be fully necrotic in the core. Taking a regular series expansion in the limit  $D_p = Q_p \rightarrow 0$ , the spheroid size can be shown to satisfy

$$S_\infty \sim \frac{D_p}{\lambda - \delta} \frac{3(n_0 + p_0 - 1)}{n_0 k_m (1, 1 - n_0)}, \tag{58}$$

where  $n_0$  is given by (57), this being valid for  $\delta < \lambda$  with  $\lambda - \delta \gg D_p$ . We note that this expression again requires that  $n_0 + p_0 - 1$  be positive, as for equation (56). Curve E in Fig. 16 is everywhere negative over the region, implying an influx of material, suggesting that the mitotic contraction factor is sufficiently high to consume all the cellular material absorbed through the surface. Formulation of a regular expansion of the form  $n \sim n_0 + n_1/D_p$  as  $D_p \rightarrow \infty$  shows that the diffusion of cellular material becomes so rapid that  $n \sim 1 - p_0$ , ensuring parity between the internal and external concentrations. However, the material flux through the surface ( $-D_p \partial p / \partial r(S_\infty) \sim \partial n_1 / \partial r(S_\infty)$ ) tends to a constant as  $D_p \rightarrow \infty$ , indicated by the levelling off of curve E in Fig. 16. Along the

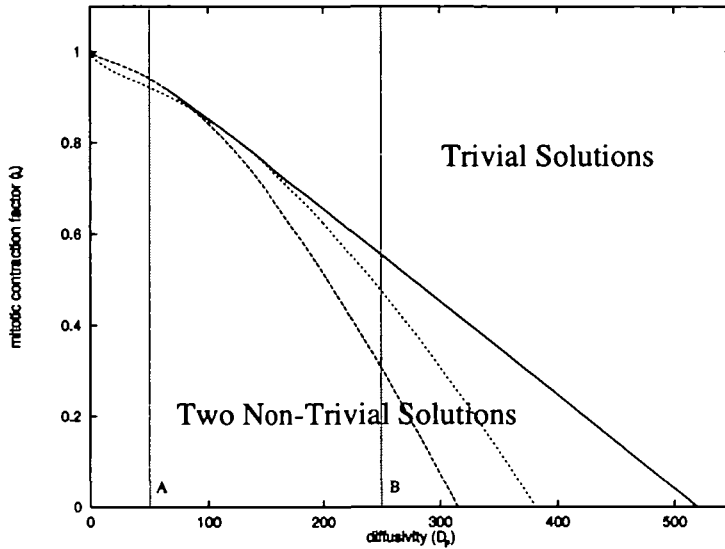


FIG. 17. The paths of (---) the steady-state/travelling-wave and (- - -) fully/partially necrotic core bifurcations in  $(D_p, \lambda)$ -parameter space. (—) The path of  $\partial\lambda/\partial S_\infty = 0$ , above which only trivial solutions exist. The paths for Fig. 18 are indicated by the dotted lines labelled A and B.

fully/partially necrotic core solution bifurcation, the saturation size is observed to increase as  $D_p$  increases, and influx turns to leakage at about  $D_p = 400$ .

The regions of existence of nontrivial solutions together with the paths of the travelling-wave/steady-state and fully/partially necrotic core solution bifurcations in  $(D_p = Q_p, \lambda)$ -parameter space are shown in Fig. 17, using the parameters given by (22) and (23) except that  $p_0 = 0$ . The solid curve tracks the bifurcation from having only the trivial solution (above the curve) to also having nontrivial solutions, and was generated by solving along the path  $\partial\lambda/\partial S_\infty = 0$ , where the upper and lower branches meet, as  $D_p$  is varied. We note that the solid curve starts at about  $D_p = 65$  due to the failure of the numerical scheme evaluating the path  $\partial\lambda/\partial S_\infty = 0$  for smaller diffusivities, the problem becoming very sensitive to the starting guesses for shooting. However, the travelling-wave/steady-state bifurcation curve (larger dashes) approximates the existence bifurcation over this region. Below the solid curve the two nontrivial solutions lie on two branches which will be termed the upper and lower branches, which meet on this solid curve. We note that the upper branch and trivial solutions are expected to be stable and the lower branch solutions to be unstable. Below the larger dashed curve, travelling-wave solutions exist and are apparently always stable. Between the two dashed curves lie the fully necrotic core solutions and we note that at a diffusivity of about  $D_p = 100$  the dashed bifurcation curves cross over, in contrast to the curves shown in Fig. 12. To the right of the cross-over point the fully necrotic core solutions always exist on the upper branch; however, to the left such solutions may exist on the lower branch. Figure 18 shows the steady-state size as a function of  $\lambda$  along the dotted paths labelled A and B in Fig. 17, the solid and dashed curves in Fig. 18 represent the upper and lower branch solutions, respectively. We note that the growth velocity of

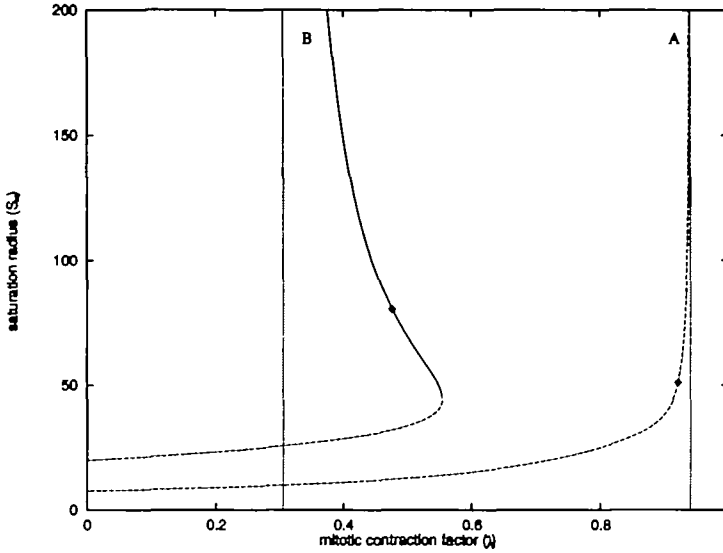


FIG. 18. Saturation size as a function of  $\lambda$  for  $D_p = Q_p = 50$  (curve A) and  $D_p = Q_p = 250$  (curve B). (—) The upper branch solution, and (---) the lower branch solution. The dotted lines, to which the other curves are asymptotes, show the position of the travelling-wave/steady-state bifurcations. (o) The fully/partially necrotic core bifurcations.

the travelling waves (not illustrated) along curves A and B descends from  $U \approx 5.72$  and  $U \approx 1.38$ , respectively, to zero at the travelling-wave/steady-state bifurcation in an almost linear fashion (similar to that shown in Fig. 13). We also note that the steady-state solutions along the upper branch are characterized by being larger and decreasing in radius as  $\lambda$  increases, whereas the saturation size increases with  $\lambda$  along the lower branch.

The results shown in the figures so far have involved the assumption that the consumption of the nutrient is independent of the local cellular material consumption, i.e. that  $\beta_2 = 0$ . In Fig. 19 the two bifurcation curves for the case  $\beta_1 = 0$  and  $\beta_2 = 0.01$  are compared with those illustrated in Fig. 12 in which  $\beta_1 = 0.01$  and  $\beta_2 = 0$ . Quantitatively there are significant differences between the curves; however, qualitatively they are similar. This type of qualitative behaviour was found to occur for a variety of choices of  $\beta_1$  and  $\beta_2$ .

In Fig. 20 the effects of the critical concentration of cellular material,  $p_c$ , on the travelling-wave/steady-state bifurcation is shown in  $(D_p = Q_p, \lambda)$ -space, with all other parameters given by (22) and (23). The decrease in  $p_c$  implies that mitosis occurs faster at a given concentration of cellular material, meaning that greater consumption is required to force saturation. In Fig. 21 a similar study performed on the effects of the external cellular material concentration  $p_0$  on the same bifurcation is shown. Increasing the external concentration reduces the readiness of the necrotic material to escape, thus requiring an increase in  $\lambda$  to compensate. However, for any  $p_0 < 1$ , leakage dominates for large enough values of  $D_p$  and the bifurcation curves eventually fall to  $\lambda = 0$ . In the case  $p_0 = 1$ , the external medium is saturated with cellular material preventing leakage of the necrotic material and the bifurcation curve carries on ascending. For the cases with  $p_0 \geq 0.1$  shown

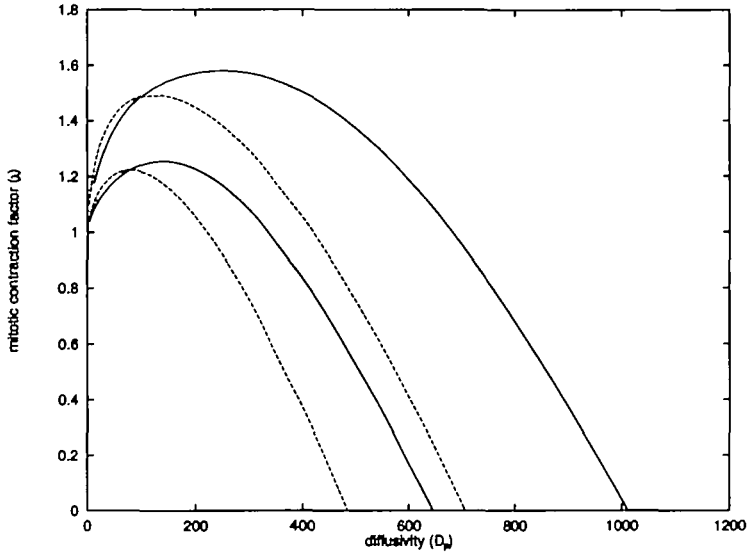


FIG. 19. A comparison of the travelling-wave/steady-state (lower curves) and fully/partially necrotic (upper curves) bifurcation curves between (—)  $\beta_1 = 0, \beta_2 = 0.01$  and (- - -)  $\beta_1 = 0.01, \beta_2 = 0$ .

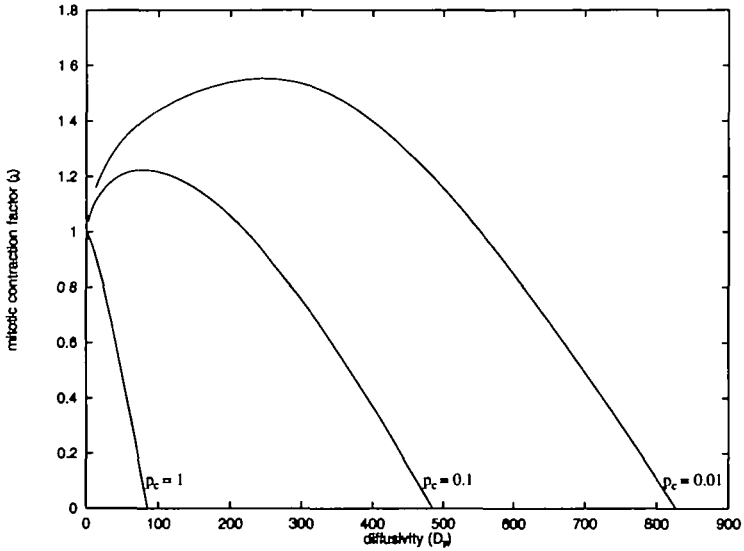


FIG. 20. The effects of the critical cellular material concentration  $p_c$  on the travelling-wave/steady-state bifurcation.

in Fig. 21, nontrivial solutions exist throughout the quarter space; however, for the case  $p_0 = 0$ , two nontrivial solutions exist over part of the quarter space.

The two bifurcations are explored in  $(\delta, \lambda)$ -space in Fig. 22, with the other parameters given by (22) and (23). As expected, increasing  $\delta$  results in increasing  $\lambda$  in order to main-

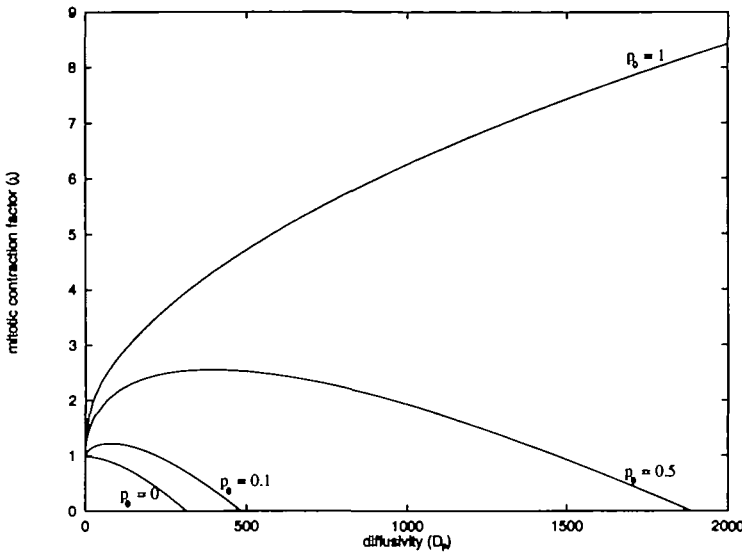


FIG. 21. The effects of the external cellular material concentration  $p_0$  on the travelling-wave/steady-state bifurcation.

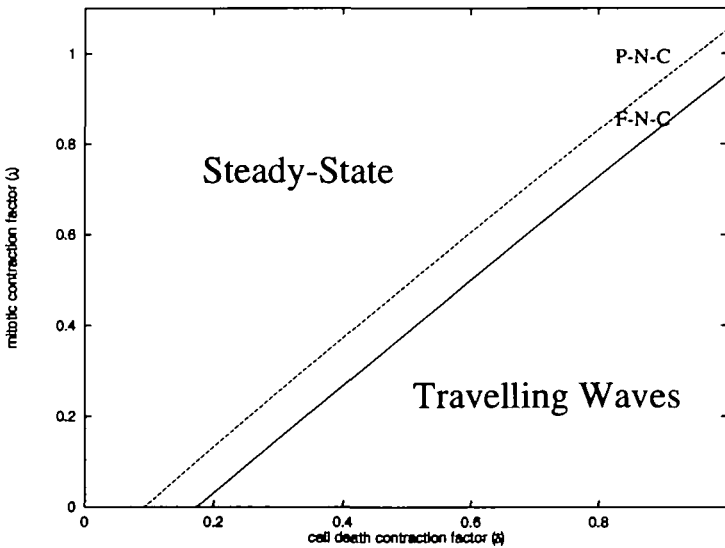


FIG. 22 The distribution of steady-state and travelling-wave solutions in  $(\delta, \lambda)$ -parameter space, showing (—) the travelling-wave/steady-state and (- - -) the fully (F-N-C)/partially (P-N-C) necrotic core bifurcations.

tain the necessary volume balance through birth and death along each of the bifurcation curves. Both curves appear to be straight and are parallel to each other, though an analytical justification for this has not yet been devised.

In Fig. 23 we drop the relation  $D_p = Q_p$ , which holds throughout the preceding ex-

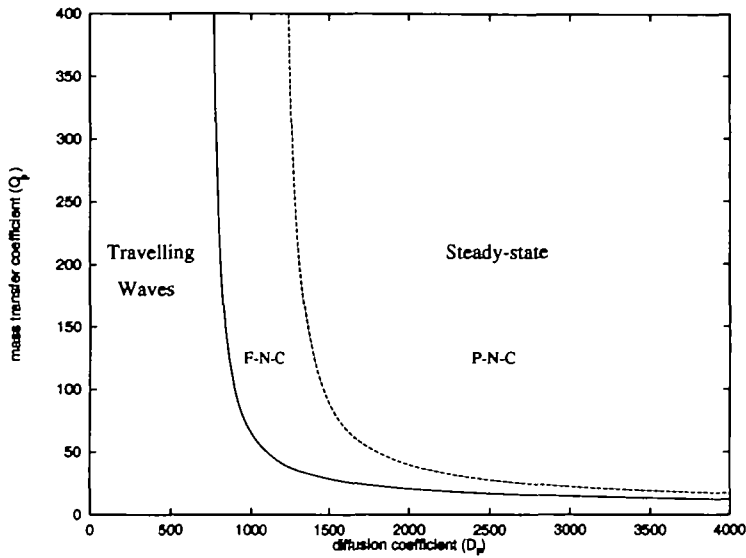


FIG. 23. The distribution of steady-state and travelling-wave solutions in  $(D_p, Q_p)$ -parameter space for the leakage-only model, showing (—) the travelling-wave/steady-state and (- - -) the fully/partially necrotic core bifurcations.

amples, and give the distribution of the two types of solutions for the leakage-only model in  $(D_p, Q_p)$ -space, the other parameters being given by (22) and  $p_0 = p_c = \lambda = 0$ . Both bifurcation curves drop sharply from their respective asymptotes, levelling off and descending to zero as  $D_p \rightarrow \infty$ . These results suggest that there exists a minimum value of  $D_p$  for which diffusion and leakage can occur at a sufficient rate to force saturation. In the limit  $D_p \rightarrow \infty$ , diffusion of the necrotic products to the surface is so rapid that, unless  $Q_p$  is sufficiently small to hinder escape, saturation of growth occurs.

Because of the relative ease of controlling the environment in which multicell spheroids are grown and of measuring gross quantities such as saturation size and viable rim width, there have been several studies reporting the effects of oxygen and glucose concentration on such features; see, for example, Bourrat-Floeck *et al.* (1991), Franko & Sutherland (1978), Hlatky *et al.* (1988), Mueller-Klieser, (1983), and Tannock & Kopelyan (1986a,b). Many of these studies found that increasing the external concentration of either glucose or oxygen results in an increased viable rim width, although Tannock & Kopelyan (1986a,b) suggest that a limit in width may be reached at which additional quantities of either oxygen or glucose have negligible effect. The results given in Bourrat-Floeck *et al.* (1991) for the case of zero external lactate concentration (lactate being a mitotic inhibitor) reveals that increasing external oxygen concentrations from 5% to 20% leads to an increase in saturation radius from about 600 to 830  $\mu\text{m}$ , with little effect on the viable rim width (about 300  $\mu\text{m}$  in both cases). This behaviour seems to correspond well with the results shown in Fig. 24, up to an external nutrient concentration of  $c(S) \approx 5$ . The parameters used for Figs. 24–26 are given by (22) with the remainder given by  $D_p = Q_p = 400$ ,  $\lambda = 1.5$ , and, again,  $p_c = p_0 = 0.1$ . We note that the dimensionless value for the external nutrient

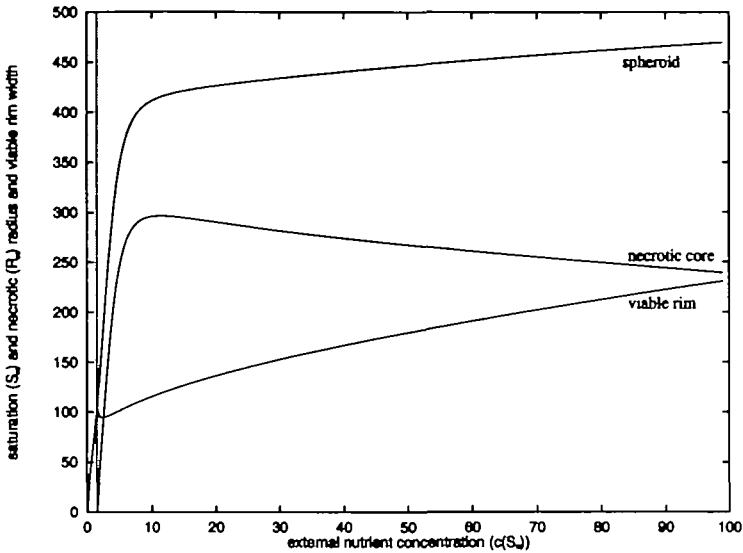


FIG. 24. Effects of the external nutrient concentration on spheroid saturation size, necrotic core radius, and viable rim width.

concentration is varied from the ‘standard’ choice of  $c(S) = 1$ , whilst the other parameters remain fixed. Here, for  $c(S) = 1$  the steady-state solution has a partially necrotic core and the fully/partially necrotic core solution bifurcation, indicated by the dotted line, occurs at about  $c(S) = 1.54$ , to the right of which are the fully necrotic core solutions. Increasing the external concentration leads to a rapid rise in both the saturation,  $S_\infty$ , and the necrotic radius,  $R_\infty$ , up to about  $c(S) = 10$ , where both curves kink, after which the saturation size continues to ascend, but more slowly, and the necrotic core radius decreases. The initial rapid increase is for the obvious reasons—there is more nutrient available, leading to greater proliferation and growth, and the diffusion rate of the cellular material is sufficiently high to supply the cells in the viable rim. This is illustrated in Fig. 25 where, noting that  $p = 1 - n$ , there is a non-negligible concentration of cellular material in the viable rim region. We note that the slight descent of the live-cell density near the surface implies the influx of material from the exterior, and it is thus the consumption of the cellular material that is the dominant process in forcing saturation in this case. Above about  $c(S) = 10$  the quantity of nutrient in the viable rim is so high that the cellular material in the central parts of the plateau region is almost completely consumed by the (now small) amount of mitosis that is occurring there, as is illustrated by the case  $c(S) = 30$  in Fig. 25. The viable rim here consists of a marked plateau of live-cell density  $n \approx 1$ , and there is a relatively high rate of mitosis occurring at the edges of the viable region, and relative quiescence in the central part, to which diffusion fails to deliver sufficient cellular material. This feature coincides with the kink in saturation size in Fig. 24, though the size continues to increase due to increased proliferation in the two regions at either edge of the viable rim. The extent of the nonuniformity of the mitotic rate in the viable rim is interesting; however, in practice the inner peak may be reduced by the presence of inhibitors produced in the core.

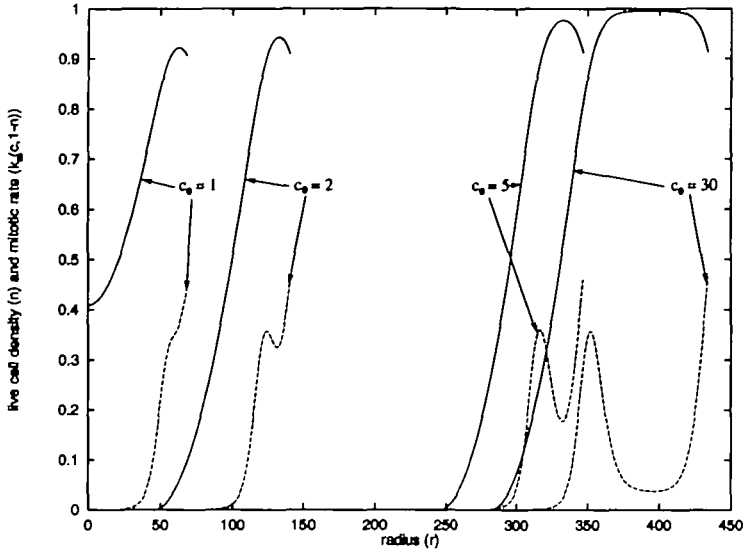


FIG. 25. (—) The live-cell density and (---) the mitotic-rate distribution of saturated spheroids for various external nutrient concentrations,  $c_0 = c(S)$ .

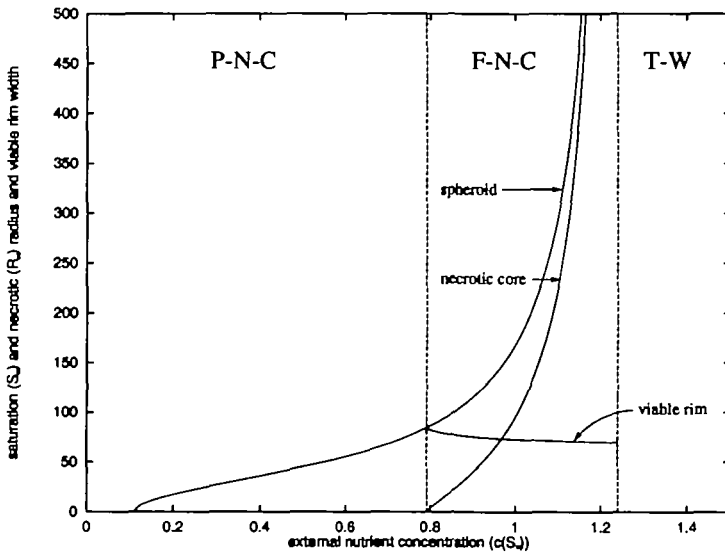


FIG. 26. Effects of the external nutrient concentration on the spheroid saturation size, necrotic core radius (position of necrotic interface), and viable rim width; fully necrotic core solutions are bounded by the dotted lines.

This response of the spheroid size to varying external nutrient concentrations is not universal, as is illustrated by Fig. 26. The parameters are given by (22) and (23), for which increasing the external nutrient concentration does, as expected, result in the increase of

saturation size, but also leads to a slight shrinkage in viable rim width. This may be a result of the reduced availability of the cellular material in the viable rim caused by its increased consumption during mitosis, which has become elevated by the higher concentrations of nutrient. This counter-intuitive behaviour has been observed in experiments on the effects of glucose concentration on thyroid carcinoma (HTh7) spheroid cultures (Acker *et al.*, 1987), with glucose concentrations well below toxic levels. Finally, as is evident from Fig. 26, there is a critical external concentration,  $c(S) = c_0^*$  say, at which the saturation size becomes zero. As  $c(S) \rightarrow c_0^{*+}$  and  $S_\infty \rightarrow 0^+$  we have  $n \sim 1 - p_0$  and  $c \sim c_0^*$  throughout the spheroid,  $c_0^*$  being such that the birth and death rate are equal, that is, such that  $a(c_0^*, p_0) = 0$ ; in this case  $c_0^* = 1/9$ .

## 6. Discussion

In existing models, rather *ad hoc* necrotic degradation terms are employed to provide the necessary volume sink to force growth saturation; such terms are intended to represent the breakdown and rapid escape of necrotic material from the spheroid. Implicit to the approach of these models is the unphysical assumption that ultimately the entire volume of the cell disappears after death, analogous to the  $\delta = 0$  case of the model of Ward & King (1997). Here we have extended that model by incorporating two biologically plausible mechanisms for the fate of the necrotic products, it being assumed that this material consists of diffusible material of non-negligible size, with utilization by the living cells and leakage being the two mechanisms for necrotic-volume loss.

Numerical solutions of both the full and long-time systems show that, given sufficient strength of the leakage and consumption mechanisms, i.e. sufficiently high values of either  $\lambda$  and  $D_p$ , growth saturation eventually occurs; otherwise growth tends toward the travelling-wave limit. Furthermore, the three-layered structure observed in experiments is also predicted. It is emphasized that the predicted growth and heterogeneity arise naturally from the model rather than being assumed *a priori*. As a consequence of the model assumptions, the steady-state solution may contain a core of zero live-cell density, reflecting complete necrosis in the core, in agreement with experimental results. The simple analysis of Section 4.5 on the long-time system of equations reveals that, except in a very special case, growth saturation occurs only if material is able to pass through the surface of the spheroid. The asymptotic analysis described in Appendix B demonstrates that, for a limiting case of the model, both the initial exponential and linear growth phases are predicted in the vanishing death-rate limit. Furthermore, the analysis provides an upper bound for the growth speed in terms of the model's parameters.

The model contains a large number of parameters, the values of several of which are unobtainable from existing data. We note that many of the parameter values are intrinsic to the cell line studied; however, environmental factors such as the external nutrient and presumably the external cellular material concentrations are experimentally controllable. In experiments, spheroid cultures eventually saturate in size if grown for a sufficient amount of time and the travelling-wave behaviour predicted by the model has not been reported. In terms of the model this suggests that the appropriate parameter values are always such that growth saturation will be achieved, although the presence of growth inhibitors and cell shedding may well be important contributory factors in preventing continual growth. However, an interesting experiment would be to study the effects of different external con-

centrations of cellular material on growth, since a sufficiently high concentration may induce continuous growth, cf. Fig. 21. The diffusion of material from the external medium into the spheroid has been extensively studied for various substances, notably nutrients and drugs; however, there has been little study of the reverse process. Analysis of the external medium for the existence of necrotic material, diffused out from the spheroid, to confirm that material leakage occurs at non-negligible levels would be useful. Experimental work on the usage of macromolecules (such as proteins, lipids and nucleic acids) by the living cells would also be interesting and such data would help ascertain the relative importance of the consumption and leakage mechanisms of necrotic-volume loss. Further experiments concerning the effects of the external nutrient concentration on saturation size would also be interesting, in order to make comparison with the types of behaviour predicted by the model in Figs. 24 and 26. Such experiments would help confirm (or otherwise) the existence of the mechanisms incorporated into the model and provide deeper understanding into the important processes that force growth saturation in spheroids.

### Acknowledgements

The first author gratefully acknowledges support by an EPSRC Earmarked Research Studentship and the second by a Nuffield Foundation Science Research Fellowship.

### REFERENCES

- ACKER, H., CARLSSON, J., HOLTERMANN, G., NEDERMAN, T., & NYLEN, T. 1987 Influence of glucose and buffer capacity in the culture medium on growth and pH in spheroids of human thyroid carcinoma and human glioma origin. *Cancer Res.* **47**, 3504–3508.
- ADAM, J. A. 1986 A simplified mathematical model of tumour growth. *Math. Biosci.* **81**, 224–229.
- BOURRAT-FLOECK, B., GROEBE, K., & MUELLER-KLIESER, W. 1991 Biological response of multicellular EMT6 spheroids to exogenous lactate. *Int. J. Cancer* **47**, 792–799.
- BYRNE, H. M. & CHAPLAIN, M. A. J. 1995 Growth of non-necrotic tumours in the presence and absence of inhibitors. *Math. Biosci.* **130**, 151–181.
- BYRNE, H. M. & CHAPLAIN, M. A. J. 1996 Growth of necrotic tumours in the presence and absence of inhibitors. *Math. Biosci.* **135**, 187–216.
- CARLSSON, J. 1977 A proliferation gradient in three-dimensional colonies of cultured human glioma cells. *Int. J. Cancer* **20**, 129–136.
- CASCIARI, J. J., SOTIRCHOS, S. V., & SUTHERLAND, R. M. 1988 Glucose diffusivity in multicellular tumour spheroids. *Cancer Res.* **48**, 3905–3909.
- CASCIARI, J. J., SOTIRCHOS, S. V., & SUTHERLAND, R. M. 1992 Mathematical modelling of micro-environment and growth in EMT6/RO multicellular tumour spheroids. *Cell Prolif.* **25**, 1–22.
- CONGAR, A. D. & ZISKIN, M. C. 1983 Growth of mammalian multicellular tumour spheroids. *Cancer Res.* **43**, 558–560.
- FOLKMAN, J. & HOCHBERG, M. 1973 Self-regulation of growth in three dimensions *J. Exp. Med.* **138**, 745–753.
- FRANKO, A. J. & SUTHERLAND, R. M. 1978 Oxygen diffusion distance and the development of necrosis in multicell spheroids. *Radiat. Res.* **79**, 439–453.
- FREYER, J. P. 1988 Role of necrosis in regulating the growth saturation of multicell spheroids. *Cancer Res.* **48**, 2432–2439.
- FREYER, J. P. & SCHOR, P. L. 1989 Regrowth kinetics of cells from different regions of multicellular spheroids of 4 cell-lines. *J. Cell. Physiol.* **138**, 384–392.
- FREYER, J. P. & SUTHERLAND, R. M. 1980 Selective dissociation and characterization of cells from different regions of multicell tumour spheroids. *Cancer Res.* **40**, 3956–3965.

- FREYER, J. P. & SUTHERLAND, R. M. 1986 Regulation of growth saturation and development of necrosis in EMT6/RO multicellular spheroids glucose and oxygen supply. *Cancer Res.* **46**, 3504–3512.
- GREENSPAN, H. P. 1972 Models for the growth of a solid tumour by diffusion. *Stud. Appl. Math.* **51**, 317–340.
- GROEBE, K. & MUELLER-KLIESER, W. 1996 On the relation between size of necrosis and diameter of tumor spheroids. *Int. J. Radiat. Onc. Biol. Phys.* **34**, 395–401.
- HLATKY, L., SUCHS, R. K., & ALPEN, E. L. 1988 Joint oxygen-glucose deprivation as the cause of necrosis in a tumour analogue. *J. Cell Phys.* **134**, 167–178.
- INCH, W. R., MCCREDIE, J. A., & SUTHERLAND, R. M. 1970 Growth of nodular carcinomas in rodents compared with multicell spheroids in tissue culture. *Growth* **34**, 271–282.
- KERR, J. F. R., SEARLE, J., HARMON, B. V., & BISHOP, C. J. 1987 Apoptosis. In: *Perspectives in Mammalian Cell Death* (C.S. Potten, ed.). Oxford University Press.
- LANDRY, J., FREYER, J. P., & SUTHERLAND, R. M. 1981 Shedding of mitotic cells from the surface of multicell spheroids during growth. *J. Cell Physiol.* **106**, 23–32.
- LANDRY, J., FREYER, J. P., & SUTHERLAND, R. M. 1982 A model for the growth of multicellular spheroids. *Cell Tiss. Kinet.* **15**, 585–594.
- LEVINE, A. E., HAMILTON, D. A., YEOMAN, L. C., BUSCH, H., & BRATTAIN, M. G. 1984 Identification of a tumour inhibitory factor in rat ascites fluid. *Biochem. Biophys. Res. Comm.* **119**, 76–82.
- MAGGELAKIS, S. A. & ADAM, J. A. 1990 Mathematical model of prevascular growth of a spheroid carcinoma. *Math. Comput. Mod.* **13**, 23–38.
- MCLEWAIN, D. L. S. & MORRIS, L. E. 1978 Apoptosis as a volume loss mechanism in mathematical models of solid tumour growth. *Math. Biosci.* **39**, 147–157.
- MUELLER-KLIESER, W. F., FREYER, J. P., & SUTHERLAND, R. M. 1983 Evidence for a major role of glucose in controlling development of necrosis in EMT6/RO multicell tumour spheroids. *Adv. Exp. Med. Biol.* **159**, 487–495.
- MUELLER-KLIESER, W. F., FREYER, J. P., & SUTHERLAND, R. M. 1985 Influence of glucose and oxygen supply conditions on the oxygenation of multicellular tumour spheroids. *Br. J. Cancer* **53**, 345–353.
- NUGENT, L. & JAIN, R. K. 1984 Extravascular diffusion in normal and neoplastic tissues. *Cancer Res.* **44**, 238–244.
- SHYMKO, R. M. & GLASS, L. 1976 Cellular and geometric control of tissue growth and mitotic instability. *J. Theor. Biol.* **63**, 355–374.
- TANNOCK, I. F. & KOPELYAN, I. 1986a Influence of glucose-concentration on growth and formation of necrosis in spheroids derived from a human bladder cancer cell-line. *Cancer Res.* **46**, 3105–3110.
- TANNOCK, I. F. & KOPELYAN, I. 1986b Variation of  $P_{O_2}$  in the growth and formation of spheroids—interaction with glucose to influence spherical growth and necrosis. *Br. J. Cancer* **53**, 823–827.
- WARD, J. P. 1997 Mathematical modelling of avascular tumour growth. PhD Thesis, Nottingham University.
- WARD, J. P. & KING, J. R. 1997 Mathematical modelling of avascular-tumour growth. *IMA J. Math. Appl. Med. Biol.* **14**, 39–69.
- WEISS, L. 1978 Some mechanisms involved in cancer cell detachment by necrotic material. *Int. J. Cancer* **22**, 196–203.

### Appendix A: Parameter values

The values for the parameters common to the model of Ward & King (1997) are discussed in the Appendix of that paper; the values for the important scaling parameters in Section 2.2 being  $V_L \approx 10^{-9} \text{ cm}^3$ , giving  $r_0 \approx 6 \times 10^{-4} \text{ cm}$ , and  $A \approx 10^{-5} \text{ s}^{-1}$ . The new parameters for the present model are  $\lambda$ ,  $D_p$ ,  $Q_p$ ,  $p_0$ ,  $p_c$ , and  $m_3$ , for which very little directly appropriate data are available from the literature. There appears to be very little experimental work investigating the effects of the cellular material, so that the appropriate kinetics for the consumption and usage of the cellular material are

unavailable; hence the values  $\lambda$ ,  $p_c$ , and  $m_3$  used in the simulations in Sections 3.2 and 5.3 are simply estimates. Experimentation geared at determining these parameters would be very valuable. The external cellular material concentration  $p_0$  could, presumably, be determined by experimental analysis of the external medium.

Since *cellular material* represents a variety of molecular species with a range of molecular masses and diffusive properties, the best choice for the value of the diffusion coefficient is unclear. However, Nugent & Jain (1984) presented several power-law expressions linking diffusion-rate coefficients with the molecular mass; these were derived from various experiments, both *in vivo* and *in vitro*. From these, although there is much variation, a value of  $D_p = 10^{-9} \text{ cm}^2 \text{ s}^{-1}$  represents material with a molecular mass,  $M_r$ , of at least  $O(10^5)$ . We note that the diffusion rate of glucose ( $M_r = 180$ ) is about  $10^{-6} \text{ cm}^2 \text{ s}^{-1}$  (for example, Casciari *et al.*, 1988), which is significantly faster than the cellular material. For the remaining parameter,  $Q_p$ , experiments examining cellular material flux across the spheroid surface are required.

Since the values of a number of these parameters have not been established, the solutions to the model are particularly instructive in revealing the dependence of the behaviour upon them. The numerical solutions discussed in Sections 3.2 and 5.3 demonstrate the high degree of sensitivity of the solutions to such parameters, both quantitatively and qualitatively. Physically relevant ranges of the parameters could be established using the criteria that the model should predict growth saturation (of a size of  $O(1 \text{ mm})$ ) with a viable rim of a few cells.

## Appendix B: Asymptotic analysis

### B.1. Introduction

The purpose of this appendix is to provide an example of how asymptotic methods can be applied to simplify the model discussed above (we note that numerous other limits, not treated here, can also be analysed by such methods) and to give a generalization to the current model of the asymptotic results of Ward & King (1997). We therefore consider the biologically plausible small death-rate limit  $\varepsilon = B/A \rightarrow 0$ , and take  $D_p = D_p^*/\varepsilon$ , and  $Q_p = Q_p^*/\varepsilon$ , where the asterisked quantities are of  $O(1)$ . These rescalings are chosen so that, in particular, the travelling-wave/steady-state bifurcation features in the limit problem. The governing system is then most conveniently written in the form

$$\frac{1}{r^2} \frac{\partial(r^2 v)}{\partial r} = [(1 - \lambda)k_m - (1 - \delta)\varepsilon \bar{k}_d]n - \frac{D_p^*}{\varepsilon} \frac{1}{r^2} \frac{\partial}{\partial r} \left( r^2 \frac{\partial n}{\partial r} \right), \quad (\text{B.1})$$

$$\frac{1}{r^2} \frac{\partial}{\partial r} \left( r^2 \frac{\partial c}{\partial r} \right) = kn, \quad (\text{B.2})$$

$$\frac{\partial n}{\partial t} + \frac{1}{r^2} \frac{\partial(r^2 n v)}{\partial r} = (k_m - \varepsilon \bar{k}_d)n, \quad (\text{B.3})$$

with

$$k_m(c, 1 - n) = \left( \frac{c^{m_1}}{c^{m_1} + c_c^{m_1}} \right) \left( \frac{(1 - n)^{m_3}}{p_c^{m_3} + (1 - n)^{m_3}} \right), \quad (\text{B.4})$$

$$k(c, 1 - n) = \beta_1 \frac{c^{m_1}}{c^{m_1} + c_c^{m_1}} + \beta_2 k_m(c, 1 - n), \quad (\text{B.5})$$

$$\bar{k}_d(c) = 1 - \frac{\sigma c^{m_2}}{c^{m_2} + c_d^{m_2}}, \quad (\text{B.6})$$

subject to (17).

**B.2.  $t = O(1)$**

There is an initial transient  $t = O(\varepsilon)$ ,  $v = O(1/\varepsilon)$  over which  $n$  drops, due to the rapid ingress of cellular material, until  $n \sim 1 - p_0$  throughout the spheroid. There follows a period of accelerated growth until quiescence, due to nutrient depletion in the core, takes effect. The accelerating growth phase can be illustrated in the limit  $\beta_1, \beta_2 \ll 1$ , so that  $c \sim 1$  for  $t \ll \ln[1/(\beta_1 + \beta_2)]$ . Here, by taking a regular expansion for small  $\varepsilon$  we find that

$$n \sim 1 - p_0 + \varepsilon \frac{(\lambda + p_0 - p_0\lambda)k_m(1, p_0)}{6D_p^*} \left( \frac{2D_p^*}{Q_p^*} S + S^2 - r^2 \right),$$

$$S \sim S_0 \exp[k_m(1, p_0)t/3]$$

for some positive constant  $S_0$ . These expansions show that in this limit the initial acceleration of growth is exponential. More generally, for the time scale  $t = O(1)$  we have to leading order

$$n \sim 1 - p_0, \tag{B.7}$$

$$\frac{1}{r^2} \frac{\partial}{\partial r} \left( r^2 \frac{\partial c}{\partial r} \right) \sim \beta \frac{c^{m_1}}{c^{m_1} + c_c^{m_1}}, \tag{B.8}$$

$$\frac{1}{r^2} \frac{\partial(r^2 v)}{\partial r} \sim \eta \frac{c^{m_1}}{c^{m_1} + c_c^{m_1}}, \tag{B.9}$$

where  $\eta = p_0^{m_3}/(p_c^{m_3} + p_0^{m_3})$  and we now define  $\beta = (1 - p_0)(\beta_1 + \beta_2\eta)$ . Hence

$$v \sim \frac{\eta}{\beta} \frac{\partial c}{\partial r}. \tag{B.10}$$

If we replace  $v$  by  $\eta v$  and  $t$  by  $t/\eta$ , we recover the  $t = O(1)$  formulation of Ward & King (1997), section 5.2, in which the constant  $q = q(\beta, m_1, c_c)$  is of the form  $q = q_0(m_1, c_c)/\beta^{1/2}$ ; the value of  $q_0$  is readily calculated for given  $m_1$  and  $c_c$ . As  $t \rightarrow \infty$ , we thus have  $S \sim q_0\eta t/\beta^{1/2}$ ; while for  $\beta \ll 1$  the growth is initially exponential. Cell death on this time scale is negligible.

The quantity  $\lambda$  plays no role in the preceding leading-order calculation; however, going to the next order we find that

$$D_p^* \frac{\partial n}{\partial r} \sim -\varepsilon(\lambda + p_0 - \lambda p_0)v, \tag{B.11}$$

which is dependent on  $\lambda$  and which can be used to quantify how much cellular material crosses the spheroid boundary and how much is consumed within the tumour. We note that the values of  $\varepsilon$  used in the numerical solutions presented elsewhere in this paper are sufficiently large, where  $\lambda$  has a significant effect on the growth behaviour.

**B.3.  $t = O(1/\varepsilon)$**

The analysis now departs more dramatically from that of Ward & King (1997). We rescale by  $t = t^*/\varepsilon$ ,  $r = r^*/\varepsilon$ ,  $S = S^*/\varepsilon$  to give at leading order in the core ( $r^* = O(S^*)$  with  $r^*/S^* < 1$ )

$$\frac{1}{r^{*2}} \frac{\partial(r^{*2}v)}{\partial r^*} = -(1 - \delta)n - \frac{D_p^*}{r^{*2}} \frac{\partial}{\partial r^*} \left( r^{*2} \frac{\partial n}{\partial r^*} \right), \tag{B.12}$$

$$\frac{\partial n}{\partial t^*} + \frac{1}{r^{*2}} \frac{\partial(r^{*2}vn)}{\partial r^*} = -n, \tag{B.13}$$

since  $c \ll 1$  and  $k_m(c, 1 - n) \ll \varepsilon$  there. Defining  $w = v + D_p^* \partial n / \partial r$  and integrating, (B.12) and (B.13) yield

$$\frac{\partial w}{\partial t} - (1 - \delta)wn = -(1 - \delta)D_p^* n \frac{\partial n}{\partial r^*} - w, \quad (\text{B.14})$$

$$\frac{1}{r^{*2}} \frac{\partial(r^{*2}w)}{\partial r^*} = -(1 - \delta)n. \quad (\text{B.15})$$

The structure in the rim ( $r^* - S^* = O(\varepsilon)$ ) is equivalent to that in Ward & King (1997), so the boundary and initial conditions (B.14) and (B.15) are

$$\begin{aligned} \text{at } r^* = 0 & \quad w = 0, \\ \text{at } r^* = S^* & \quad n = 1 - p_0, \quad \frac{dS^*}{dt^*} = w - D_p^* \frac{\partial n}{\partial r^*} + \frac{q_0 \eta}{\beta^{1/2}}, \\ \text{at } t^* = 0 & \quad S^* = 0. \end{aligned} \quad (\text{B.16})$$

The second condition at  $r^* = S^*$  arises because the net growth rate of the spheroid is determined by the contraction in the core (giving the first two terms on the right-hand side) and the rate of mitosis in the rim (giving the  $q_0$  term); the tumour reaches the steady state if these two rates come to balance. It can be shown by rescaling that the behaviour of (B.14)–(B.16) depends on  $q_0$  and  $D_p^*$  only through the combination  $q_0/\sqrt{D_p^*}$ . We also note that  $\lambda$  again does not appear in the leading-order problem but does determine how much cellular material enters or leaves the tumour.

The moving-boundary problem (B.14)–(B.16) cannot be solved analytically, but it is possible to determine the location of the travelling-wave/steady-state bifurcation. Steady states satisfy

$$w = -D_p^* \frac{(1 - \delta)n}{1 - (1 - \delta)n} \frac{dn}{dr^*}, \quad (\text{B.17})$$

with

$$\frac{D_p^*}{r^{*2}} \frac{d}{dr^*} \left( r^{*2} \frac{n}{1 - (1 - \delta)n} \frac{dn}{dr^*} \right) = n. \quad (\text{B.18})$$

As indicated above, to locate the bifurcation (corresponding to the limit  $S_\infty^* \rightarrow \infty$ ) we solve the one-dimensional version of (B.18); namely,

$$D_p^* \frac{d}{dz} \left( \frac{n}{1 - (1 - \delta)n} \frac{dn}{dz} \right) = n, \quad (\text{B.19})$$

where  $z = r^* - S_\infty^*$ , subject to

$$\begin{aligned} \text{as } z \rightarrow -\infty & \quad n \rightarrow 0, \\ \text{at } z = 0 & \quad n = 1 - p_0, \quad \frac{D_p^*}{1 - (1 - \delta)(1 - p_0)} \frac{dn}{dz} = \frac{q_0 \eta}{\beta^{1/2}}, \end{aligned} \quad (\text{B.20})$$

in fact, because (B.19) is degenerate, we have  $n \equiv 0$  for  $z \leq -z_0$  for some  $z_0 > 0$ . Equation (B.19) can be integrated to yield

$$\frac{D_p^* n^2}{2[1 - (1 - \delta)n]^2} \left( \frac{dn}{dz} \right)^2 = -\frac{n^2}{2(1 - \delta)} - \frac{n}{(1 - \delta)^2} - \frac{1}{(1 - \delta)^3} \ln[1 - (1 - \delta)n], \quad (\text{B.21})$$

and, by imposing the boundary conditions at  $z = 0$ , we find that the travelling-wave/steady state bifurcation is located at

$$\frac{q_0}{\sqrt{D_p^*}} = \frac{\left( 2\beta \left\{ -\ln[1 - (1 - \delta)(1 - p_0)] - (1 - \delta)(1 - p_0) - (1 - \delta)^2(1 - p_0)^2/2 \right\} \right)^{1/2}}{(1 - \delta)^{3/2} \eta(1 - p_0)}. \quad (\text{B.22})$$

For larger values of  $q_0/\sqrt{D_p^*}$ , a travelling-wave will occur, while for smaller values the solution will

evolve to a steady state. As an aside, we note that, much more generally, the problem governing a bifurcation between travelling waves and steady states may be significantly more easy to address analytically than general travelling-wave and steady-state solutions, since the appropriate formulation is in some respects simpler than either.

As  $\delta \rightarrow 1$  or  $p_0 \rightarrow 1$ , we have

$$\frac{q_0}{\sqrt{D_p^*}} \sim \frac{\left[\frac{2}{3}\beta(1-p_0)\right]^{\frac{1}{2}}}{\eta}. \tag{B.23}$$

Further progress is possible for  $\delta = 1$ , when  $w \equiv 0$  and (B.12) can be reduced to a degenerate reaction–diffusion equation

$$\frac{\partial n}{\partial t^*} = \frac{D_p^*}{r^{*2}} \frac{\partial}{\partial r^*} \left( r^{*2} n \frac{\partial n}{\partial r^*} \right) - n. \tag{B.24}$$

The solution to (B.19) is then

$$n = \frac{(z+z_0)_+^2}{6D_p^*}, \quad z_0 = [6D_p^*(1-p_0)]^{\frac{1}{2}}. \tag{B.25}$$

More significantly, we can also locate the fully/partially necrotic core bifurcation; when  $\delta = 1$ , equation (B.18) has a closed-form solution

$$n = \frac{r^{*2}}{10D_p^*}, \tag{B.26}$$

and imposing the boundary conditions yields

$$S_\infty^* = [10D_p^*(1-p_0)]^{1/2}, \quad q_0/\sqrt{D_p^*} = [2\beta(1-p_0)/5]^{1/2}/\eta.$$

The solution (B.26) satisfies the conditions required to be on the bifurcation curve, having  $n = 0$  at  $r^* = 0$ , so for  $\delta = 1$  we have a partially necrotic steady-state for

$$\frac{q_0}{\sqrt{D_p^*}} < \frac{[2\beta(1-p_0)/5]^{1/2}}{\eta},$$

fully necrotic for

$$\frac{[2\beta(1-p_0)/5]^{1/2}}{\eta} < \frac{q_0}{\sqrt{D_p^*}} < \frac{[2\beta(1-p_0)/3]^{1/2}}{\eta}$$

and a travelling wave for

$$\frac{q_0}{\sqrt{D_p^*}} > \frac{[2\beta(1-p_0)/3]^{1/2}}{\eta}.$$